Journal of Guidance, Control, and Dynamics, Volume 41, Issue 4, 2018, pp. 888-903
DOI:10.2514/1.G003071

Nonlinear Analytical Uncertainty Propagation for Relative Motion near J_2-Perturbed, Elliptic Orbits

Zhen Yang*, Ya-zhong Luo†,

National University of Defense Technology, 410073 Changsha, People's Republic of China

Vaios Lappas‡, and Antonios Tsourdos§

Cranfield University, Cranfield, England MK43 0AL, United Kingdom

Abstract: An analytical uncertainty propagation method based on state transition tensors (STTs) has been developed for satellite relative motion near J_2-perturbed, elliptic orbits. The STTs used to propagate the relative state uncertainty are derived by adding a correction into the original STTs for propagating relative state. A new set of transitive STTs is further derived in order to propagate uncertainties for relative motion with abrupt state jumps, e.g. impulsive maneuvers executing on any of the two satellites. The nonlinear analytical solution for propagating the first two moments and the probability density function are formulated by combining the STTs with a Gaussian mixture model. Numerical results show that the proposed method outperforms the linear covariance method and provides good agreement with Monte Carlo simulations on nonlinear, non-Gaussian uncertainty propagation. Moreover, as the STTs can be analytically computed and account for the J_2-perturbation, the proposed uncertainty propagator is computationally efficient, which will be potentially useful for onboard conjunction analysis in satellites formulation flying mission.

I. Introduction

Nowadays, increasing attentions have been paid to satellite formation flying, as that the use of multiple satellites in a close formation can have numerous advantages over one single, larger spacecraft [1]. However, the formation flying introduces new problems in maintaining the formation geometry and in preventing inadvertent collisions between satellites as a result of uncertainties in neighboring satellites' states or possible failures of one of the satellite. The equation describing satellites relative motion is a theoretical basis to the issue of maintaining formation geometry, thus numerous relative-motion equations have been studied in the past years. The first linear relative-motion kinematics for near-circular and elliptic reference orbits are the well-known Clohessy-Wiltshire (C-W) equations [2] and Tschauner-Hempel (T-H) equations [3], respectively. Schweighart and Sedwick [4] expanded on the C-W model by including first-order secular effects of J_2-perturbation,

* PhD Candidate, College of Aerospace Science and Engineering; yangzhen@nudt.edu.cn.
† Professor, College of Aerospace Science and Engineering; luoyz@nudt.edu.cn, Senior Member AIAA.
‡ Professor, School of Aerospace, Transport and Manufacturing; vaios.lappas@cranfield.ac.uk, Senior Member AIAA.
§ Director of Research, School of Aerospace, Transport and Manufacturing; a.tsourdos@cranfield.ac.uk, Member AIAA.

and Yamanaka and Ankersen [5] improved the T-H equations by giving an unperturbed time-dependent solution. These models [2-5] employed rectilinear coordinates to describe the satellites' relative states. In contrast, more recent works have derived the relative-motion equations based on the relative orbital elements (ROE), since the ROE varies slowly with the time and allows for including perturbations more conveniently. Gim and Alfriend [6, 7] first developed a relative-motion equation to include the first-order secular and osculating J_2-perturbation in arbitrarily eccentric orbits, in which better accuracy were also obtained by synthetically using the ROE and curvilinear coordinates, instead of using rectilinear coordinates. Recently, this J_2-perturbed model had been extended to the complete zonal gravitational problem [8]. Moreover, D'Amico et al. [9] formulated the relative motion of two spacecraft in arbitrarily eccentric orbits perturbed by J_2 and differential drag by using three different definitions of ROE, Schaub [10, 11] proposed a general method to the modelling and control of relative orbit geometry through ROE, and Biria and Russell [12] derived an analytical relative-motion equations including J_2 and J_3 via Vinti's Intermediary. Although the effects of orbital eccentricity and perturbation had been well-cooperated in these research efforts [4-12], they were just linear approximations to the naturally-nonlinear orbital dynamics, which would be insufficient for problems with large separation distance between satellites. To overcome this shortcoming, additional works had been done to account for the effects of nonlinear terms. Gurfil and Kasdin [13] established a methodology to obtain arbitrary high-order approximations to the relative motion between spacecraft by utilizing the Cartesian configuration space in conjunction with classical orbital elements. Sengupta and Vadali [14] developed a second-order analytical propagation of relative motion near perturbed, elliptic orbits. To sum up, a comprehensive survey of these relative models can be found in a recent work by Sullivan et al. [15].

On the other hand, for the problem of preventing inadvertent collisions among formation-flying satellites, it is necessary to propagate the relative state uncertainty, for the objective of collision probability computation [16, 17] or relative reachable domain analysis [18]. Orbital uncertainty propagation was usually addressed by linear covariance (LinCov) analysis [19, 20] or nonlinear Monte Carlo (MC) simulations [21, 22]. The linear methods are very efficient through simplifying the problem, but their accuracy decreases in highly nonlinear systems or long-duration propagations. Conversely, MC simulations provide high-precision statistics, but are computationally expensive. To avoid these shortcomings, some nonlinear analytical or semi-analytical techniques had been developed in recent years, such as the unscented transformation (UT) method [23], the polynomial chaos (PC) method [24, 25], the state transition tensors (STTs) method [26, 27], the differential algebraic (DA) technique [28, 29], the Gaussian mixture model (GMM) [30-32], and the method of solving Fokker–Planck equation (FPE) [33, 34]. The UT method [23] delivers an efficient, second-

order approximation only for the first two moments of the mapped statistical distributions by using less than $2n+1$ sigma-points. In comparison to UT, the PC method [24, 25] can provide more accurate information on higher-order moments and the entire PDF, however, it suffers from the problem of dimensionality. The STTs-based methods [26, 27] can analytically propagate uncertainty and requires no random samples once the STTs are integrated along the nominal trajectory. However, high-order derivatives of the governing dynamics need to be computed for these methods, which will be very complex for high-fidelity dynamic systems. Alternatively, the DA technique [28, 29] supplies a tool to automatically compute the derivatives of functions within a computerized environment. Recently, Sun and Kumar [33, 34] proposed a tensor decomposition method for orbital uncertainty propagation, which is a numerical result for direct solution of FPE. However, solving FPE is extremely difficult for high-dimension systems, e.g. the 6-dimensional orbital dynamics system. Instead, the GMM method [30-32] tends to approximate a non-Gaussian PDF by using a finite sum of weighted Gaussian density functions. It decouples a large uncertainty propagation problem into many small problems, which is an effective methodology to represent a non-Gaussian distribution and to reduce the effects of nonlinearity in dynamics. Moreover, some hybrid methods had also been developed through integrating the advantages of different uncertainty propagators, such as the combined GMM and STTs method [35, 36], and the combined GMM and PC method [37]. Recently, a detailed review of orbital uncertainty propagation was given by Luo and Yang [38].

The nonlinear uncertainty propagators mentioned above [23-34] mainly focus on the propagation of absolute states uncertainties of satellites, which is usually performed by ground control centers. However, the uncertainty propagation for formation-flying satellites needs to be carried out onboard [16]. Thus, analytical algorithms are required so that satellite onboard computers having low computational capability can perform necessary computations efficiently. To address this issue, linear analytical uncertainty propagators for satellite relative motion had been developed based on the linearized relative motion and white Gaussian process noises [17, 39]. However, these approaches relied on an assumption of circular chief orbit so that the linear relative dynamic models (e.g., C-W equations) can be used. As an improvement, Lee et al. [16] further proposed an analytical, closed-form uncertainty propagation method for relative motion near general elliptic orbits. However, these analytical uncertainty propagators [16, 17, 39] did not account for any practical perturbations (e.g. the Earth oblateness and atmospheric drag). In fact, based on the LinCov technique [20], all the state transition matrices (STMs) employed in the linear relative-motion models [2-12] can be directly used to propagate the relative state uncertainty. However, as will be revealed in this study, the higher-order nonlinear solution for propagating relative state (e.g., [14]) cannot be directly used for propagate the relative state uncertainty. In addition, the STMs-based LinCov methods are

only defined to linearly compute the mean and covariance matrix of the relative state uncertainty, which may be inadequate for long-duration, non-Gaussian uncertainty propagation problems.

Therefore, this study motivates to develop a nonlinear, analytical method for the long-duration, non-Gaussian uncertainty propagation of satellite relative motion. Based on the analytical solutions proposed by Sengupta et al. [14] and Gim and Alfriend [6], a set of second-order analytical STTs for propagating the difference of relative motion is derived. These STTs are then applied to nonlinearly propagate the mean and covariance matrix of relative state uncertainty. Considering the fact that a Gaussian distribution will become non-Gaussian distribution when mapped by the inherently nonlinear relative dynamics, a method combining the GMM and STTs is developed to analytically propagate the PDF of the relative state uncertainty. Based on the proposed STTs and the library data of splitting the univariate Gaussian distribution [32], we can analytically evaluate the uncertainty of the relative state between two satellites at any time of interest without any numerical integration, in which the effects of impulsive maneuvers and their uncertainties can also be taken into account.

This manuscript is organized as follows. Section II gives the basic dynamical models and introduces the uncertainty propagation problem. Section III derives the second-order state transition of relative state difference based on the nonlinear solution for satellite relative motion. In Sec. IV, the nonlinear covariance propagation method is developed by using covariance analysis technique. Section V investigates the nonlinear propagation of PDF using a method combining the GMM and STTs. Numerical results and comparisons are presented in Sec. VI, and conclusions are finally drawn in Sec. VII.

II. Problem Statement

In order to formulate the nonlinear analytical uncertainty propagator with J_2-perturbation, the stochastic orbital dynamics and a general uncertainty propagation problem are first introduced in this section.

A. Orbital Dynamics

Orbital dynamic problem entailing uncertainty can be expressed by the Itô stochastic differential equation [40],

$$d\boldsymbol{x}(t) = \boldsymbol{f}(\boldsymbol{x},t)dt + \boldsymbol{W}(t)d\boldsymbol{\beta}(t) \tag{1}$$

where $\boldsymbol{x}\in\mathbb{R}^n$ is the random state vector, $\boldsymbol{\beta}(t)\in\mathbb{R}^m$ is a m-dimensional Brownian motion process with zero mean and covariance $\boldsymbol{\Theta}(t)$. The vector function $\boldsymbol{f}(\boldsymbol{x},t)$ captures the deterministic part of the dynamics, and $\boldsymbol{W}(t)$ is an $n\times m$ matrix characterizing the diffusion. The initial condition uncertainty is determined by the probability density function (PDF) $p(\boldsymbol{x}_0,t_0)$, assumed known.

For the satellite's motion concerned in this study, the deterministic part $\boldsymbol{f}(\boldsymbol{x},t)$ of the dynamics can be given by an ordinary differential equation (ODE) [19]

$$\boldsymbol{f}(\boldsymbol{x},t)=\ddot{\boldsymbol{r}}=-\mu\frac{\boldsymbol{r}}{r^3}+\boldsymbol{a}_{per}+\boldsymbol{u} \tag{2}$$

where $\boldsymbol{x}\in\mathbb{R}^n$ denotes the satellite's state with a dimensionality of n=6, $\boldsymbol{x}=[\boldsymbol{r},\boldsymbol{v}]^T$, $\boldsymbol{r}$ and $\boldsymbol{v}$ are the respective position and velocity vectors described in the central body's inertial coordinate system (ICS); μ is the central body's gravitational constant, $r=\|\boldsymbol{r}\|$, $\|\cdot\|$ denotes the Euclid norm of a vector; $\boldsymbol{a}_{per}$ is the perturbation acceleration caused by factors such as the non-spherical gravity and the atmospheric drag, only J_2-perturbation is considered in this study. $\boldsymbol{u}$ is the thrust acceleration vector. If the impulsive maneuver is assumed, the thrust acceleration can be approximated in terms of K impulses as follows:

$$\boldsymbol{u}(t)=\sum_{k=1}^{K}\Delta\boldsymbol{v}_k\delta(t-t_k) \tag{3}$$

where K is the number of impulses, t_k is the k^{th} maneuver time, and $\delta(t-t_k)$ is the Dirac delta function.

Relative motion is conveniently described in a local vertical/local horizontal (LVLH) frame, which is attached to the center of mass of the *chief* satellite (also called the *leader* or *target*), the x-axis is aligned with the Chief orbit radius, the z-axis is along the orbit normal, and the y-axis completes the right-handed system. Let's denote the position of the *deputy* satellite (also called the *follower* or *chaser*) in the Chief LVLH frame as $\boldsymbol{\rho}=[\delta x,\delta y,\delta z]^T$, where δx, δy, and δz denote the components of the position vector along the radial, transverse, and normal directions, respectively.

Considering the central body's J_2-perturbation only, in the Chief LVLH frame, the relative motion of Deputy satisfies the following dynamics [14]

$$\begin{cases}\delta\ddot{x}-2\dot{\theta}\delta\dot{y}-\dot{\theta}^2\delta x-\ddot{\theta}\delta y=\dfrac{-\mu(r+\delta x)}{[(r+\delta x)^2+\delta y^2+\delta z^2]^{3/2}}+\dfrac{\mu}{r^2}+a_{J2x}+u_x\\ \delta\ddot{y}+2\dot{\theta}\delta\dot{x}-\dot{\theta}^2\delta y+\ddot{\theta}\delta x=\dfrac{-\mu\delta y}{[(r+\delta x)^2+\delta y^2+\delta z^2]^{3/2}}+a_{J2y}+u_y\\ \delta\ddot{z}=\dfrac{-\mu\delta z}{[(r+\delta x)^2+\delta y^2+\delta z^2]^{3/2}}+a_{J2z}+u_z\end{cases} \tag{4}$$

where $\theta=\omega+f$ is Chief's argument of latitude, r is the distance from central gravity to Chief, $\boldsymbol{a}_{J2}$ and $\boldsymbol{u}$ are the J_2-perturbation and thrust acceleration described in the Chief LVLH frame. Equation (4) has no analytical solution unless some approximations are assumed.

B. Uncertainty Propagation Problem

Given an initial state $\boldsymbol{x}(t_0)$ and its associated uncertainty which is usually described by a mean $\boldsymbol{m}(t_0)$ and a covariance matrix $\boldsymbol{C}(t_0)$, or a PDF $p(\boldsymbol{x}_0, t_0)$, the issue of uncertainty propagation is to predict the state and its statistical properties (moments or PDF) at a future time, *t*.

For a given dynamical system that satisfies Eq. (1), the time evolution of a PDF $p(\boldsymbol{x}, t)$ over $\boldsymbol{x}$ at time *t* is described by the FPE [40]:

$$\frac{\partial p(\boldsymbol{x},t)}{\partial t} = -\sum_{i=1}^{n} \frac{\partial}{\partial x^i}[p(\boldsymbol{x},t)\boldsymbol{f}^i(\boldsymbol{x},t)] + \frac{1}{2}\sum_{i=1}^{n}\sum_{j=1}^{n} \frac{\partial^2}{\partial x^i \partial x^j}\{p(\boldsymbol{x},t)[\boldsymbol{W}(t)\boldsymbol{\Theta}(t)\boldsymbol{W}^T(t)]^{ij}\} \quad (5)$$

The FPE is a partial differential equation that governs the time evolution of a PDF. Hence, the solution of the FPE provides a complete statistical description of a trajectory depends on Eq. (1). However, uncertainty propagation is always an extremely difficult process if we prefer to a complete statistical description, because it generally requires one to solve partial differential equations such as the FPE in Eq. (5) or to carry out particle-type studies such as MC simulations. The solving of FPE in orbital mechanics is a difficult task, primarily because the underlying FPE is defined in a relatively high dimensional state–space (6-D) and is driven by the nonlinear perturbed Keplerian dynamics, as shown in Eq. (2). Moreover, although the MC method has high precision on uncertainty propagation and is easy to implement, it requires a large number of random samples for obtaining convergent statistics, which makes it computationally expensive.

Therefore, in order to efficiently quantify uncertainty within given range of the accuracy requirement, approximation methods are usually required, in which the Gaussian distribution assumption of uncertainty and the local linearization of the dynamics are commonly used. The statistics of a Gaussian distribution can be completely described by the first two moments, and the Gaussian distribution structure will remain unchanged under linear mapping. Thus, only the first two moments are required propagating under these assumptions. For a given uncertain state vector $\boldsymbol{x}$, its mean ($\boldsymbol{m}$) and covariance matrix ($\boldsymbol{C}$) can be defined as,

$$\begin{aligned} \boldsymbol{m} &= E[\boldsymbol{x}] \\ \boldsymbol{C} &= E\left[(\boldsymbol{x}-\boldsymbol{m})(\boldsymbol{x}-\boldsymbol{m})^{\mathrm{T}}\right] = E[\boldsymbol{x}\boldsymbol{x}^{\mathrm{T}}] - \boldsymbol{m}\boldsymbol{m}^{\mathrm{T}} \end{aligned} \quad (6)$$

where $E[\cdot]$ represents the expectation operator.

Considering no process noise $d\boldsymbol{\beta}(t)$ in Eq. (1), linearizing the dynamics $\boldsymbol{f}(\boldsymbol{x}, t)$ along a nominal trajectory $\hat{\boldsymbol{x}}(t)$, and assuming that the uncertain state $\boldsymbol{x}(t)$ belongs to Gaussian distribution, then the uncertainty propagation problem can be simplified to propagate the mean and covariance matrix only, i.e.,

$$\boldsymbol{m}(t) = \boldsymbol{\Phi}(t, t_0)\boldsymbol{m}_0, \quad \boldsymbol{C}(t) = \boldsymbol{\Phi}(t, t_0)\boldsymbol{C}_0\boldsymbol{\Phi}(t, t_0)^{\mathrm{T}} \quad (7)$$

where $\boldsymbol{m}_0 = \boldsymbol{m}(t_0)$, $\boldsymbol{C}_0 = \boldsymbol{C}(t_0)$, and $\boldsymbol{\Phi}$ is the STM which can be analytically computed or numerically integrated along the nominal trajectory $\hat{\boldsymbol{x}}(t)$, i.e.,

$$\dot{\boldsymbol{\Phi}} = \left.\frac{\partial \boldsymbol{f}(t,\boldsymbol{x})}{\partial \boldsymbol{x}}\right|_{\boldsymbol{x}=\hat{\boldsymbol{x}}} \boldsymbol{\Phi}, \quad \boldsymbol{\Phi}(t_0,t_0) = \boldsymbol{I} \tag{8}$$

The linear uncertainty propagation in Eqs. (7) and (8) is well-known as linear covariance (LinCov) analysis technique [20]. This technique is similar with the predict step of a Kalman filter or an extent Kalman filter. It had been widely used in spaceflight missions [20] as it simplifies the problem and has a high computation efficiency. However, its accuracy drops down for highly nonlinear dynamics and long-term uncertainty propagation. As shown in Eqs. (2) and (4), the orbital dynamics is naturally nonlinear. The structure of Gaussian distribution will no longer be preserved when mapping it through a nonlinear dynamical system. To solve this issue, this study investigates a nonlinear analytical method for long-term, non-Gaussian orbital uncertainty propagation under J_2-perturbation. A nonlinear covariance propagation method is first formulated based on the analytical solution of propagating relative state difference. This nonlinear covariance method is then incorporated into the GMM method to propagate the PDF of a non-Gaussian distribution.

III. State Transition Tensors for Relative Motion

Sengupta et al. [14] proposed a second order analytical solution for the relative motion near elliptic orbits. Combining this nonlinear solution with Gim and Alfriend's linear analytical solution of relative motion near J_2-perturbed, elliptic orbits [6], Sengupta et al. [14] further derived a second-order analytical solution for the relative motion near J_2-perturbed, elliptic orbits. However, this J_2-perturbed nonlinear solution only presented a nonlinear mapping from the mean relative orbital elements to the normalized relative state, as shown in Eqs. (46-48) of [14], and we thought that a small typo might exist in Eq. (46) of [14].

In this section, a more complete second-order analytical solution for the relative motion near J_2-perturbed, elliptical orbits is derived based on the similar concept in [14]. However, the second-order analytical solution derived here is a little different from that in [14]. Furthermore, in order to construct a nonlinear uncertainty propagation for satellite relative motion, the obtained second-order analytical solution for relative motion has been revised and extended to propagate the relative state difference in Sec. III.D.

A. STTs for Nonlinear, Unperturbed Relative Motion

Let $\boldsymbol{E} = [a, e, i, \Omega, \omega, f]$ denote the satellite's classic orbital elements, where a is the semi-major axis, e is the eccentricity, i is the inclination, Ω is the right ascension of the ascending node, ω is the

argument of periapsis, and f is the true anomaly. The orbital elements-set $\boldsymbol{E}$ is singular for circular orbits, $e = 0$. To avoid this singularity, a set of modified orbital elements can be defined as, $\boldsymbol{e} = [a, \theta, i, q_1, q_2, \Omega]$, where $q_1 = e\cos\omega$, $q_2 = e\sin\omega$, and $\theta = \omega + f$ is the argument of latitude. Moreover, it is defined that the relative orbital elements are: $\delta\boldsymbol{e} = [\delta a, \delta\theta, \delta i, \delta q_1, \delta q_2, \delta\Omega]$, and the normalized relative orbital elements are $\delta\boldsymbol{\alpha} = [\delta a/a, \delta\theta, \delta i, \delta q_1, \delta q_2, \delta\Omega]$. In the Chief LVLH frame, it is defined that the time-dependent relative state is: $\delta\boldsymbol{x}(t) = [\boldsymbol{\rho}, \dot{\boldsymbol{\rho}}]^T$, and the normalized relative state is: $\delta\boldsymbol{x}(\theta) = [\boldsymbol{\rho}, \boldsymbol{\rho}']^T$, where the symbol $(\dot{})$ denote the first derivative with respect to time, and the symbol $()'$ denote the first derivative with respect to θ. Based on these definitions, the relative motion between two satellites can be described using the relative states: $\delta\boldsymbol{x}(t)$ and $\delta\boldsymbol{x}(\theta)$, or using the relative orbital elements: $\delta\boldsymbol{e}$ and $\delta\boldsymbol{\alpha}$.

By considering no J_2-perturbation ($\boldsymbol{a}_{J2} = \boldsymbol{0}$) and no thrust acceleration ($\boldsymbol{u} = \boldsymbol{0}$) in Eq. (4), Sengupta et al. [14] proposed a second-order analytical propagation of the normalized relative orbital elements $\delta\boldsymbol{\alpha}$, i.e.,

$$\delta\boldsymbol{\alpha}(\theta_f) = \boldsymbol{G}(\theta_f, \theta_0)\delta\boldsymbol{\alpha}(\theta_0) + \frac{1}{2}\boldsymbol{H}(\theta_f, \theta_0) \otimes \delta\boldsymbol{\alpha}(\theta_0) \otimes \delta\boldsymbol{\alpha}(\theta_0) \tag{9}$$

and a second-order analytical mapping from the normalized relative orbital elements $\delta\boldsymbol{\alpha}(\theta)$ to the normalized relative state $\delta\boldsymbol{x}(\theta)$, i.e.,

$$\delta\boldsymbol{x}(\theta) = \boldsymbol{P}(\theta)\delta\boldsymbol{\alpha}(\theta) + \frac{1}{2}\boldsymbol{Q}(\theta) \otimes \delta\boldsymbol{\alpha}(\theta) \otimes \delta\boldsymbol{\alpha}(\theta) \tag{10}$$

where $\boldsymbol{G} \in \mathbb{R}^{6\times6}$ and $\boldsymbol{P} \in \mathbb{R}^{6\times6}$ are STMs, $\boldsymbol{H} \in \mathbb{R}^{6\times6\times6}$ and $\boldsymbol{Q} \in \mathbb{R}^{6\times6\times6}$ are the third-order STTs, and the operator $\otimes$ denotes the Kronecker tensor product. Since a matrix is also a second-order STT, both the STM and the third-order STT will be denoted as STTs. The STTs ($\boldsymbol{G}$, $\boldsymbol{P}$, $\boldsymbol{H}$, $\boldsymbol{Q}$) were given in [14]. Combining Eq. (9) with Eq. (10), a second-order analytical propagation of the normalized relative state $\delta\boldsymbol{x}(\theta)$ was also derived in [14].

B. STM for Linear, Perturbed Relative Motion

Considering the J_2-perturbation in Eq. (4), Gim and Alfriend [6] derived a linear solution of propagating the mean relative orbital elements $\delta\bar{\boldsymbol{e}}$,

$$\delta\bar{\boldsymbol{e}}(t_f) = \bar{\boldsymbol{\phi}}_{\boldsymbol{e}}(t_f, t_0)\delta\bar{\boldsymbol{e}}(t_0) \tag{11}$$

a linear mapping between the osculating relative orbital elements $\delta\boldsymbol{e}(t)$ and the mean relative orbital elements $\delta\bar{\boldsymbol{e}}(t)$,

$$\delta\boldsymbol{e}(t) = \bar{\boldsymbol{D}}(t)\delta\bar{\boldsymbol{e}}(t) \tag{12}$$

and a linear mapping between the relative state $\delta\boldsymbol{X}(t)$ and the osculating relative orbital elements $\delta\boldsymbol{e}(t)$,

$$\delta \boldsymbol{X}(t) = \boldsymbol{\Sigma}(t)\delta \boldsymbol{e}(t) \tag{13}$$

where $\delta\boldsymbol{X}(t) = [\delta x,\ \delta v_x,\ \delta y,\ \delta v_y,\ \delta z,\ \delta v_z]$, a horizontal bar, i.e. $\bar{\square}$, over a variable denotes that this variable is calculated using Chief's mean orbital elements $\bar{\boldsymbol{e}}(t)$, the STMs ($\boldsymbol{\Sigma}$, $\bar{\boldsymbol{D}}$, $\bar{\boldsymbol{\phi}}_{\boldsymbol{e}}$) were given in [6].

Specifically, the relative states ($\delta\boldsymbol{x}(t)$, $\delta\boldsymbol{X}(t)$, $\delta\boldsymbol{x}(\theta)$) and the relative orbital elements ($\delta\boldsymbol{e}(t)$, $\delta\boldsymbol{\alpha}(t)$) satisfy the following equations,

$$\begin{aligned} \delta \boldsymbol{x}(t) &= \boldsymbol{\Pi}\delta \boldsymbol{X}(t) = \boldsymbol{T}(\theta)\delta \boldsymbol{x}(\theta) \\ \delta \boldsymbol{e}(t) &= \boldsymbol{\Gamma}(t)\delta \boldsymbol{\alpha}(t) \end{aligned} \tag{14}$$

where the transformation matrices, $\boldsymbol{\Pi}$, $\boldsymbol{T}$ and $\boldsymbol{\Gamma}$, were given in [14].

C. STTs for Relative State in J_2-Perturbed, Elliptic Orbits

In the nonlinear solution of relative motion, in order to account for J_2-perturbation, it is necessary to use $\bar{\boldsymbol{\phi}}_{\boldsymbol{e}}(\theta_f,\theta_0)$ in Eq. (11) instead of $\boldsymbol{G}(\theta_f,\theta_0)$ in Eq. (9), and to use $\boldsymbol{\Sigma}(\theta)$ in Eq. (13) instead of $\boldsymbol{P}(\theta)$ in Eq. (10). Considering the transformations in Eq. (14), $\bar{\boldsymbol{\phi}}_{\boldsymbol{e}} = \boldsymbol{\Gamma}^{-1}\boldsymbol{G}\boldsymbol{\Gamma}$ and $\boldsymbol{\Sigma} = \boldsymbol{\Pi}^{-1}\boldsymbol{T}\boldsymbol{P}\boldsymbol{\Gamma}^{-1}$ were satisfied in the absence of J_2-perturbation.

Substituting Eqs. (11), (12) and (14) into Eq. (9), a nonlinear propagation from the mean relative orbital elements to the osculating orbital elements under J_2-perturbation can be obtained as,

$$\begin{aligned} \delta\boldsymbol{\alpha}(\theta_f) &= \boldsymbol{\Gamma}^{-1}(\theta_f)\bar{\boldsymbol{D}}(\theta_f)\bar{\boldsymbol{\phi}}_{\boldsymbol{e}}(\theta_f,\theta_0)\bar{\boldsymbol{\Gamma}}(\theta_0)\delta\bar{\boldsymbol{\alpha}}(\theta_0) \\ &\quad + \frac{1}{2}\boldsymbol{\Gamma}^{-1}(\theta_f)\bar{\boldsymbol{D}}(\theta_f)\bar{\boldsymbol{\Gamma}}(\theta_f)\bar{\boldsymbol{H}}(\theta_f,\theta_0)\otimes\delta\bar{\boldsymbol{\alpha}}(\theta_0)\otimes\delta\bar{\boldsymbol{\alpha}}(\theta_0) \end{aligned} \tag{15}$$

By substituting Eq. (15) into Eq. (10), and comprising linear and quadratic terms only, then a second-order propagation from the mean relative orbital elements $\delta\bar{\boldsymbol{\alpha}}(\theta_0)$ to the normalized relative state $\delta\boldsymbol{x}(\theta_f)$ can be derived as

$$\begin{aligned} \delta\boldsymbol{x}(\theta_f) &= \boldsymbol{A}\bar{\boldsymbol{\phi}}_{\boldsymbol{e}}(\theta_f,\theta_0)\bar{\boldsymbol{\Gamma}}(\theta_0)\delta\bar{\boldsymbol{\alpha}}(\theta_0) + \frac{1}{2}\boldsymbol{Q}(\theta_f)\otimes\left[\boldsymbol{B}\delta\bar{\boldsymbol{\alpha}}(\theta_0)\right]\otimes\left[\boldsymbol{B}\delta\bar{\boldsymbol{\alpha}}(\theta_0)\right] \\ &\quad + \frac{1}{2}\boldsymbol{A}\bar{\boldsymbol{\Gamma}}(\theta_f)\bar{\boldsymbol{H}}(\theta_f,\theta_0)\otimes\delta\bar{\boldsymbol{\alpha}}(\theta_0)\otimes\delta\bar{\boldsymbol{\alpha}}(\theta_0) \\ \boldsymbol{A} &= \boldsymbol{T}^{-1}(\theta_f)\boldsymbol{\Pi}\boldsymbol{\Sigma}(\theta_f)\bar{\boldsymbol{D}}(\theta_f),\ \ \boldsymbol{B} = \boldsymbol{\Gamma}^{-1}(\theta_f)\bar{\boldsymbol{D}}(\theta_f)\bar{\boldsymbol{\phi}}_{\boldsymbol{e}}(\theta_f,\theta_0)\bar{\boldsymbol{\Gamma}}(\theta_0) \end{aligned} \tag{16}$$

By considering only the average effect of J_2-perturbation in the second-order terms of Eq. (16), i.e. using the mean relative orbital elements in the last two terms of Eq. (16), Sengupta et al. [14] presented another nonlinear propagation from the mean relative orbital elements $\delta\bar{\boldsymbol{\alpha}}(\theta_0)$ to the normalized relative state $\delta\boldsymbol{x}(\theta_f)$, i.e.,

$$\begin{aligned} \delta\boldsymbol{x}(\theta_f) &= \boldsymbol{T}^{-1}(\theta_f)\boldsymbol{\Pi}\boldsymbol{\Sigma}(\theta_f)\bar{\boldsymbol{D}}(\theta_f)\bar{\boldsymbol{\phi}}_{\boldsymbol{e}}(\theta_f,\theta_0)\bar{\boldsymbol{\Gamma}}(\theta_0)\delta\bar{\boldsymbol{\alpha}}(\theta_0) \\ &\quad + \frac{1}{2}\boldsymbol{F}\bar{\boldsymbol{H}}(\theta_f,\theta_0)\otimes\delta\bar{\boldsymbol{\alpha}}(\theta_0)\otimes\delta\bar{\boldsymbol{\alpha}}(\theta_0) + \frac{1}{2}\bar{\boldsymbol{Q}}(\theta_f)\otimes\left[\boldsymbol{\Xi}\delta\bar{\boldsymbol{\alpha}}(\theta_0)\right]\otimes\left[\boldsymbol{\Xi}\delta\bar{\boldsymbol{\alpha}}(\theta_0)\right] \end{aligned} \tag{17}$$

where $\boldsymbol{\Xi} = \bar{\boldsymbol{\Gamma}}^{-1}(\theta_f)\bar{\boldsymbol{\phi}}_{\boldsymbol{e}}(\theta_f,\theta_0)\bar{\boldsymbol{\Gamma}}(\theta_0)$. It should be noted that, in the Eq. (46) of [14], the matrix $\boldsymbol{F}$ in Eq. (17) was given as, $\boldsymbol{F} = \bar{\boldsymbol{\Sigma}}(\theta_f)$. We thought that this formulation of $\boldsymbol{F}$ matrix ($\boldsymbol{F} = \bar{\boldsymbol{\Sigma}}(\theta_f)$) was incorrect, because some transformations between different relative orbital elements and relative states were missed. This might be a small typo for the Eq. (46) of [14]. Considering the coordinate transformations in Eq. (14), the correct expression of $\boldsymbol{F}$ matrix can be obtained as $\boldsymbol{F} = \bar{\boldsymbol{T}}^{-1}(\theta_f)\boldsymbol{\Pi}\bar{\boldsymbol{\Sigma}}(\theta_f)\bar{\boldsymbol{\Gamma}}(\theta_f)$.

As illustrated in Sec. VI.A, the accuracy of Eq. (16) is slightly better than that of Eq. (17) in satellite relative motion propagation. Therefore, in the following context, we only use Eq. (16) to further derive a complete second-order state transition of relative motion by using the time-dependent relative state $\boldsymbol{x}(t)$.

Rewriting Eq. (16) to be a brief expression, we obtain,

$$\begin{aligned}
&\delta\boldsymbol{x}(\theta_f) = \tilde{\boldsymbol{P}}(\theta_f,\theta_0)\delta\bar{\boldsymbol{\alpha}}(\theta_0) + \frac{1}{2}\tilde{\boldsymbol{Q}}(\theta_f,\theta_0)\otimes\delta\bar{\boldsymbol{\alpha}}(\theta_0)\otimes\delta\bar{\boldsymbol{\alpha}}(\theta_0)\\
&\tilde{\boldsymbol{P}}(\theta_f,\theta_0) = \boldsymbol{A}\bar{\boldsymbol{\phi}}_{\boldsymbol{e}}(\theta_f,\theta_0)\bar{\boldsymbol{\Gamma}}(\theta_0)\\
&\tilde{Q}^{ijk}(\theta_f,\theta_0) = A^{il}\bar{\Gamma}^{lm}(\theta_f)\bar{H}^{mjk}(\theta_f,\theta_0) + Q^{ilm}(\theta_f)B^{lj}B^{mk}
\end{aligned} \tag{18}$$

where the Einstein summation notation is employed for all the dummy variables (i, j, k, l, m), e.g., for a dummy variable m, $\Phi^{im}x^m = \sum_{m=1}^{6}\Phi^{im}x^m$.

Letting $\theta_f = \theta_0$, the following approximate solution for a given relative state $\delta\boldsymbol{x}(\theta_0)$ can be obtained by applying a reversion of series on (18),

$$\begin{aligned}
\delta\bar{\boldsymbol{\alpha}}(\theta_0) = {}& \tilde{\boldsymbol{P}}^{-1}(\theta_0,\theta_0)\delta\boldsymbol{x}(\theta_0) - \frac{1}{2}\tilde{\boldsymbol{P}}^{-1}(\theta_0,\theta_0)\tilde{\boldsymbol{Q}}(\theta_0,\theta_0)\otimes\\
&\left[\tilde{\boldsymbol{P}}^{-1}(\theta_0,\theta_0)\delta\boldsymbol{x}(\theta_0)\right]\otimes\left[\tilde{\boldsymbol{P}}^{-1}(\theta_0,\theta_0)\delta\boldsymbol{x}(\theta_0)\right]
\end{aligned} \tag{19}$$

where the initial conditions for calculating $\tilde{\boldsymbol{P}}(\theta_0,\theta_0)$ and $\tilde{\boldsymbol{Q}}(\theta_0,\theta_0)$ using Eq. (18) are: $\bar{\boldsymbol{\phi}}_{\boldsymbol{e}}(\theta_0,\theta_0) = \mathbf{I}_6$ and $\bar{H}^{mjk}(\theta_0,\theta_0) = 0$, $\mathbf{I}_n$ is an n-dimension identical matrix.

Substituting Eq. (19) into Eq. (18), the analytical nonlinear propagation of the normalized relative state $\delta\boldsymbol{x}(\theta)$ can be derived as,

$$\begin{aligned}
&\delta\boldsymbol{x}(\theta_f) = \tilde{\boldsymbol{\Phi}}(\theta_f,\theta_0)\delta\boldsymbol{x}(\theta_0) + \frac{1}{2}\tilde{\boldsymbol{\Psi}}(\theta_f,\theta_0)\otimes\delta\boldsymbol{x}(\theta_0)\otimes\delta\boldsymbol{x}(\theta_0)\\
&\tilde{\Phi}^{ij}(\theta_f,\theta_0) = \tilde{P}^{il}(\theta_f,\theta_0)[\tilde{\boldsymbol{P}}^{-1}(\theta_0,\theta_0)]^{lj}\\
&\tilde{\Psi}^{ijk}(\theta_f,\theta_0) = \tilde{Q}^{ilm}(\theta_f,\theta_0)[\tilde{\boldsymbol{P}}^{-1}(\theta_0,\theta_0)]^{lj}[\tilde{\boldsymbol{P}}^{-1}(\theta_0,\theta_0)]^{mk}\\
&\qquad -\tilde{\Phi}^{il}(\theta_f,\theta_0)\tilde{Q}^{lmn}(\theta_0,\theta_0)[\tilde{\boldsymbol{P}}^{-1}(\theta_0,\theta_0)]^{mj}[\tilde{\boldsymbol{P}}^{-1}(\theta_0,\theta_0)]^{nk}
\end{aligned} \tag{20}$$

Moreover, substituting Eq. (14) into Eq. (20), the nonlinear analytical propagation of the time-dependent relative state $\boldsymbol{x}(t)$ can be finally obtained as

$$\begin{aligned}
&\delta \boldsymbol{x}(t_f) = \boldsymbol{\Phi}(t_f,t_0)\delta \boldsymbol{x}(t_0) + \frac{1}{2}\boldsymbol{\Psi}(t_f,t_0)\otimes\delta \boldsymbol{x}(t_0)\otimes\delta \boldsymbol{x}(t_0)\\
&\Phi^{ij}(t_f,t_0) = T^{il}(t_f)\tilde{\Phi}^{lm}(t_f,t_0)[\boldsymbol{T}^{-1}(t_0)]^{mj}\\
&\Psi^{ijk}(t_f,t_0) = T^{il}(t_f)\tilde{\Psi}^{lmn}(t_f,t_0)[\boldsymbol{T}^{-1}(t_0)]^{mj}[\boldsymbol{T}^{-1}(t_0)]^{nk}
\end{aligned} \tag{21}$$

where the STTs ($\boldsymbol{\Phi},\boldsymbol{\Psi}$) can be analytically calculated using Chief initial orbital element $\boldsymbol{e}(t_0)$ and the propagation time $\Delta t = t_f - t_0$.

D. STTs for Relative State Difference in J_2-Perturbed, Elliptic Orbits

Denote Deputy's nominal relative state as $\delta\hat{\boldsymbol{x}}(t)$, Eq. (21) gives an analytical, second-order state transition of relative state $\delta \boldsymbol{x}(t)$ in J_2-perturbed, elliptic orbits. However, it cannot be directly used for propagating the relative state difference, i.e. $d\boldsymbol{x}(t) = \delta \boldsymbol{x}(t) - \delta\hat{\boldsymbol{x}}(t)$. In order to propagate the satellite's relative state uncertainty, we need to derive a nonlinear mapping of the relative state difference which can be regarded as a random realization of the relative state uncertainty.

Assuming that there is a difference $d\boldsymbol{x}(t)$ on the nominal relative state $\delta\hat{\boldsymbol{x}}(t)$, then its real relative state $\delta \boldsymbol{x}(t)$ can be expressed as

$$\delta \boldsymbol{x}(t) = \delta\hat{\boldsymbol{x}}(t) + d\boldsymbol{x}(t) \tag{22}$$

where the difference $d\boldsymbol{x}(t)$ can be regarded as a random realization of Deputy's relative state uncertainty.

Substituting Eq. (22) into Eq. (21), we obtain

$$\begin{aligned}
\delta\hat{\boldsymbol{x}}_f + d\boldsymbol{x}_f = {}& \boldsymbol{\Phi}_{(t_f,t_0)}\delta\hat{\boldsymbol{x}}_0 + \frac{1}{2}\boldsymbol{\Psi}_{(t_f,t_0)}\otimes\delta\hat{\boldsymbol{x}}_0\otimes\delta\hat{\boldsymbol{x}}_0\\
&+ \boldsymbol{\Phi}_{(t_f,t_0)}d\boldsymbol{x}_0 + \frac{1}{2}\boldsymbol{\Psi}_{(t_f,t_0)}\otimes d\boldsymbol{x}_0\otimes d\boldsymbol{x}_0\\
&+ \frac{1}{2}\boldsymbol{\Psi}_{(t_f,t_0)}\otimes\delta\hat{\boldsymbol{x}}_0\otimes d\boldsymbol{x}_0 + \frac{1}{2}\boldsymbol{\Psi}_{(t_f,t_0)}\otimes d\boldsymbol{x}_0\otimes\delta\hat{\boldsymbol{x}}_0
\end{aligned} \tag{23}$$

where $\delta\hat{\boldsymbol{x}}_i = \delta\hat{\boldsymbol{x}}(t_i)$ and $d\boldsymbol{x}_i = d\boldsymbol{x}(t_i)$ for i = 0, f. Comparing Eq. (23) with the propagation of $\delta\hat{\boldsymbol{x}}(t_0)$ using Eq. (21), the propagation of relative state difference $d\boldsymbol{x}(t_0)$ can be expressed as

$$\begin{aligned}
&d\boldsymbol{x}_f = \hat{\boldsymbol{\Phi}}_{(t_f,t_0)}d\boldsymbol{x}_0 + \frac{1}{2}\boldsymbol{\Psi}_{(t_f,t_0)}\otimes d\boldsymbol{x}_0\otimes d\boldsymbol{x}_0\\
&\hat{\Phi}^{ij}_{(t_f,t_0)} = \Phi^{ij}_{(t_f,t_0)} + \frac{1}{2}(\Psi^{ikj}_{(t_f,t_0)} + \Psi^{ijk}_{(t_f,t_0)})\delta\hat{x}^k_0
\end{aligned} \tag{24}$$

Here, $\hat{\boldsymbol{\Phi}},\boldsymbol{\Psi}$ is the STTs for propagating the relative state difference. Comparing Eq. (24) with the second-order solution in Eq. (21), the propagation of relative state difference depends on both the relative state difference and the nominal relative state. That is, comparing to the propagation of relative state, the propagation of relative state difference requires a correction on the first-order STT

$\boldsymbol{\Phi}_{(t_f,t_0)}$.

IV. Nonlinear Covariance Propagation of Relative State Uncertainty

This section develops a nonlinear method for propagating the first-two moments of relative state uncertainty by using the derived STTs in Eq. (24). A nonlinear covariance propagation for free relative motion (i.e., no maneuvers on both satellites) is first formulated in Sec. IV.A. Then, it is extended to more complex scenarios that consider maneuvers executing on Deputy or Chief. For these scenarios, a set of transitive STTs needs to be derived by considering the abrupt state jumps caused by maneuvers, as shown in Secs. IV.B and IV.C.

A. Covariance Propagation for Free Relative Motion

Substituting Eq. (24) into Eq. (6), the nonlinear propagation of mean and covariance matrix for the initial relative state uncertainty can be obtained as

$$\begin{aligned} m^i(t_f) &= \widehat{\Phi}^{ia}_{(t_f,t_0)} E[dx_0^a] + \frac{1}{2}\Psi^{iab}_{(t_f,t_0)} E[dx_0^a dx_0^b] \\ C^{ij}(t_f) &= \widehat{\Phi}^{ia}_{(t_f,t_0)} \widehat{\Phi}^{jb}_{(t_f,t_0)} E[dx_0^a dx_0^b] \\ &\quad + \frac{1}{2}\left[\widehat{\Phi}^{ia}_{(t_f,t_0)}\Psi^{jbc}_{(t_f,t_0)} + \widehat{\Phi}^{jb}_{(t_f,t_0)}\Psi^{ibc}_{(t_f,t_0)}\right] E[dx_0^a dx_0^b dx_0^c] \\ &\quad + \frac{1}{4}\Psi^{iab}_{(t_f,t_0)}\Psi^{jcd}_{(t_f,t_0)} E[dx_0^a dx_0^b dx_0^c dx_0^d] - m^i(t_f)m^j(t_f) \end{aligned} \tag{25}$$

Assuming that the initial relative state uncertainty is Gaussian distribution, then the third and fourth original moments can be computed using the mean and covariance matrix [26]:

$$\begin{aligned} E[dx_0^a] &= m_0^a \\ E[dx_0^a dx_0^b] &= C_0^{ab} + m_0^a m_0^b \\ E[dx_0^a dx_0^b dx_0^c] &= m_0^a m_0^b m_0^c + m_0^a C_0^{bc} + m_0^b C_0^{ac} + m_0^c C_0^{ab} \\ E[dx_0^a dx_0^b dx_0^c dx_0^d] &= m_0^a m_0^b m_0^c m_0^d + C_0^{ab}C_0^{cd} + C_0^{ac}C_0^{bd} + C_0^{ad}C_0^{bc} \\ &\quad + m_0^a m_0^b C_0^{cd} + m_0^a m_0^c C_0^{bd} + m_0^a m_0^d C_0^{bc} + m_0^b m_0^c C_0^{ad} + m_0^b m_0^d C_0^{ac} + m_0^c m_0^d C_0^{ab} \end{aligned} \tag{26}$$

For the sake of simplicity, the nonlinear covariance propagation in Eqs. (25) and (26) is denoted as

$$\left[\boldsymbol{m}_f, \boldsymbol{C}_f\right] = STT\left[\boldsymbol{m}_0, \boldsymbol{C}_0; \hat{\boldsymbol{e}}_0, \delta\hat{\boldsymbol{x}}_0, \widehat{\boldsymbol{\Phi}}_{(t_f,t_0)}, \boldsymbol{\Psi}_{(t_f,t_0)}\right] \tag{27}$$

where $\boldsymbol{m}_i = \boldsymbol{m}(t_i)$ and $\boldsymbol{C}_i = \boldsymbol{C}(t_i)$ for $i = 0, f$, $\hat{\boldsymbol{e}}_0 = \hat{\boldsymbol{e}}(t_0)$ is Chief nominal orbital element, and $\delta\hat{\boldsymbol{x}}_0$ is the initial nominal relative state. $\hat{\boldsymbol{e}}_0$ and $\delta\hat{\boldsymbol{x}}_0$ are used to compute the STTs $\widehat{\boldsymbol{\Phi}}_{(t_f,t_0)}$ and $\boldsymbol{\Psi}_{(t_f,t_0)}$.

Equation (24) gives a nonlinear analytical propagation of relative state difference for "free relative motion", i.e., neither Deputy nor Chief executes any maneuver ($\boldsymbol{u} = \boldsymbol{0}$) and thus the relative

trajectory is consecutive. However, this consecutive mapping cannot be directly used to propagate the relative state difference $d\boldsymbol{x}(t)$ while there is an abrupt state jump in any of the satellites, e.g., the Deputy or Chief executes an impulsive maneuver at time t ($t_0 < t < t_f$). If only the first-order solution is considered in Eq. (24), the STM $\widehat{\boldsymbol{\Phi}}$ in (24) is naturally transitive, i.e. $\widehat{\boldsymbol{\Phi}}_{(t_f,t_0)} = \widehat{\boldsymbol{\Phi}}_{(t_f,t)}\widehat{\boldsymbol{\Phi}}_{(t,t_0)}$. However, the STT $\boldsymbol{\Psi}$ is not transitive when the second-order solution is considered. In order to keep the second-order precision in the propagation of relative state uncertainty, transitive STTs are derived in the following two sections for scenarios with Deputy and Chief maneuvering, respectively.

B. Covariance Propagation with Deputy Maneuvering

We first consider the scenario with Deputy executing impulsive maneuvers, i.e. $t_k, \Delta\boldsymbol{v}_k$ (k = 1, 2, …, K, $t_0 \le t_1 <\ldots< t_K \le t_f$), during the propagation period $[t_0, t_f]$. Here, the impulses $\Delta\boldsymbol{v}_k$ are described in the Chief LVLH frame at t_k. The relative trajectory is divided into (K+1) segments by the K impulses on Deputy. Because an abrupt state jump exists in the relative trajectory at each t_k, the STTs $\widehat{\boldsymbol{\Phi}}, \boldsymbol{\Psi}$ in Eq. (24) need to be computed independently for every segmented trajectory after adding the impulse $\Delta\boldsymbol{v}_k$ into Deputy velocity.

Let's consider that the impulsive maneuver $\Delta\boldsymbol{v}_k$ (k = 1, 2, …, K) is also uncertain, then the real impulse can be written as: $\Delta\boldsymbol{v}_k = \Delta\hat{\boldsymbol{v}}_k + d\boldsymbol{v}_k$. Here, $\Delta\hat{\boldsymbol{v}}_k$ is the nominal impulse, and $d\boldsymbol{v}_k = \delta\Delta\boldsymbol{v}_k$ is a random realization of the impulse uncertainty. Thus, the post-maneuver nominal relative state $\delta\hat{\boldsymbol{x}}_1^+$ and the post-maneuver relative state difference $d\boldsymbol{x}_1^+$ can be expressed as

$$\begin{aligned} \delta\hat{\boldsymbol{x}}_1^+ &= \delta\hat{\boldsymbol{x}}_1 + \hat{\boldsymbol{x}}_{v1}, \quad \hat{\boldsymbol{x}}_{v1} = [\boldsymbol{0}_3, \Delta\hat{\boldsymbol{v}}_1]^T \\ d\boldsymbol{x}_1^+ &= d\boldsymbol{x}_1 + d\boldsymbol{x}_{v1}, \quad d\boldsymbol{x}_{v1} = [\boldsymbol{0}_3, d\boldsymbol{v}_1]^T \end{aligned} \tag{28}$$

where the superscript "+" denotes the state after an impulse.

Briefly, by substituting Eqs. (24) and (28) into Eq. (6) repeatedly, the relative state uncertainty can be segmentally propagated to the final time along the (K+1) segments of relative trajectories, i.e.,

$$\begin{aligned} m_{k+1}^i &= \widehat{\Phi}_{(t_{k+1},t_k)}^{ia}(m_k^a)^+ + \frac{1}{2}\Psi_{(t_{k+1},t_k)}^{iab}\left[(C_k^{ab})^+ + (m_k^a)^+(m_k^b)^+\right] \\ C_{k+1}^{ij} &= \widehat{\Phi}_{(t_{k+1},t_k)}^{ia}\widehat{\Phi}_{(t_{k+1},t_k)}^{jb}\left[(C_k^{ab})^+ + (m_k^a)^+(m_k^b)^+\right] \\ &\quad + \frac{1}{2}\left[\widehat{\Phi}_{(t_{k+1},t_k)}^{ia}\Psi_{(t_{k+1},t_k)}^{jbc} + \widehat{\Phi}_{(t_{k+1},t_k)}^{jb}\Psi_{(t_{k+1},t_k)}^{ibc}\right](E[dx_k^a dx_k^b dx_k^c])^+ \\ &\quad + \frac{1}{4}\Psi_{(t_{k+1},t_k)}^{iab}\Psi_{(t_{k+1},t_k)}^{jcd}(E[dx_k^a dx_k^b dx_k^c dx_k^d])^+ - m_{k+1}^i m_{k+1}^j \end{aligned} \tag{29}$$

where k = 0, 1, …, K, $t_{K+1} = t_f$; $d\boldsymbol{x}_0^+ = d\boldsymbol{x}_0$, $d\boldsymbol{x}_k^+ = d\boldsymbol{x}_k + d\boldsymbol{x}_{vk}$ and $d\boldsymbol{x}_{vk} = [\boldsymbol{0}_3, d\boldsymbol{v}_k]^T$; $\boldsymbol{m}_0^+ = \boldsymbol{m}_0$, $\boldsymbol{m}_k^+ = \boldsymbol{m}_k + \boldsymbol{m}_{vk}$, $\boldsymbol{C}_0{}^+ = \boldsymbol{C}_0$, and $\boldsymbol{C}_k^+ = \boldsymbol{C}_k + \boldsymbol{C}_{vk}$. $\boldsymbol{m}_{vk} = \left[\boldsymbol{0}_3, E[d\boldsymbol{v}_k]\right]^T$, and $E[d\boldsymbol{v}_k]$ is the mean of the k^{th} impulse uncertainty. Let $\boldsymbol{C}(d\boldsymbol{v}_k)$ be the covariance matrix of the k^{th} impulse uncertainty, then $\boldsymbol{C}_{vk}$ can be expressed as $\boldsymbol{C}_{vk} = \left[\boldsymbol{0}_{3\times3}, \boldsymbol{0}_{3\times3}; \boldsymbol{0}_{3\times3}, \boldsymbol{C}(d\boldsymbol{v}_k)\right]$. In Eq. (26), let $\boldsymbol{m}_0 = \boldsymbol{m}_k^+$ and $\boldsymbol{C}_0 = \boldsymbol{C}_k^+$, then the third and fourth moments at post-maneuver times, i.e. $(E[dx_k^a dx_k^b dx_k^c])^+$ and $(E[dx_k^a dx_k^b dx_k^c dx_k^d])^+$, can be calculated.

The uncertainty propagation in Eq. (29) is simple and easy-to-implement. However, as the numerical results shown in Sec. VI, it is low-accuracy on propagating the relative state uncertainty, because the relative state uncertainty $\boldsymbol{m}_k, \boldsymbol{C}_k$ (k = 1, …, K) in Eq. (29) may become very large when dispersed by the former segments of trajectories (e.g. k < 3), which makes the second-order solution of Eq. (29) become insufficient to approximate the real solution for the latter segments of trajectories (i.e. k > 3), and thus large truncation errors may be produced. To avoid this problem, a set of transitive STTs is derived as follows.

For the sake of clearance, we first consider that only one impulsive maneuver $t_1, \Delta\boldsymbol{v}_1$ is executed by Deputy, and the final time is set to be t_2. That is to propagate the initial relative state difference $d\boldsymbol{x}(t_0)$ from t_0 to t_2, during which the first impulse is performed at t_1.

According to Eq. (24), the propagation of relative state difference in the first segmented trajectory can be expressed as

$$d\boldsymbol{x}_1 = \widehat{\boldsymbol{\Phi}}_{(t_1,t_0)} d\boldsymbol{x}_0 + \frac{1}{2}\boldsymbol{\Psi}_{(t_1,t_0)} \otimes d\boldsymbol{x}_0 \otimes d\boldsymbol{x}_0 \tag{30}$$

Similarly with Eq. (30), the propagation of relative state difference in the second segmented trajectory can be expressed as

$$\begin{aligned} d\boldsymbol{x}_2 &= \widehat{\boldsymbol{\Phi}}_{(t_2,t_1)} d\boldsymbol{x}_1^+ + \frac{1}{2}\boldsymbol{\Psi}_{(t_2,t_1)} \otimes d\boldsymbol{x}_1^+ \otimes d\boldsymbol{x}_1^+ = dA + dB + dC \\ \widehat{\Phi}^{ij}_{(t_2,t_1)} &= \Phi^{ij}_{(t_2,t_1)} + \frac{1}{2}\left[\Psi^{ikj}_{(t_2,t_1)} + \Psi^{ijk}_{(t_2,t_1)}\right]\left[\delta\hat{\boldsymbol{x}}_1^+\right]^k \end{aligned} \tag{31}$$

where the STTs $\boldsymbol{\Phi}, \boldsymbol{\Psi}$ is computed based on Eq. (21) with the Chief's nominal orbital element $\hat{\boldsymbol{e}}_1$, and the terms dA, dB and dC are obtained by substituting Eq. (28) into Eq. (31), i.e.,

$$\begin{aligned} dA &= \widehat{\boldsymbol{\Phi}}_{(t_2,t_1)} d\boldsymbol{x}_1 + \frac{1}{2}\boldsymbol{\Psi}_{(t_2,t_1)} \otimes d\boldsymbol{x}_1 \otimes d\boldsymbol{x}_1 = \widehat{\boldsymbol{\Phi}}_{(t_2,t_0)} d\boldsymbol{x}_0 + \frac{1}{2}\boldsymbol{\Psi}_{(t_2,t_0)} \otimes d\boldsymbol{x}_0 \otimes d\boldsymbol{x}_0 \\ dB &= \widehat{\boldsymbol{\Phi}}_{(t_2,t_1)} d\boldsymbol{x}_{v1} + \frac{1}{2}\boldsymbol{\Psi}_{(t_2,t_1)} \otimes d\boldsymbol{x}_{v1} \otimes d\boldsymbol{x}_{v1} \\ dC &= \boldsymbol{\Psi}_{(t_2,t_1)} \otimes d\boldsymbol{x}_1 \otimes d\boldsymbol{x}_{v1} = \widehat{\boldsymbol{\Phi}}_{(t_1,t_0)} \otimes \boldsymbol{\Psi}_{(t_2,t_1)} \otimes d\boldsymbol{x}_0 \otimes d\boldsymbol{x}_{v1} \end{aligned} \tag{32}$$

Here, $d\boldsymbol{x}_1$ is eliminated from the expression of $d\boldsymbol{x}_2$ by substituting Eq. (30) into Eq. (32) and comprising linear and quadratic terms only. Let $\bar{\boldsymbol{\Phi}}_{(t_2,t_0)}$ and $\boldsymbol{\Psi}_{(t_2,t_0)}$ denote the transitive STTs from t_0 to t_2, then they are expressed as

$$\begin{aligned}\bar{\Phi}^{ij}_{(t_2,t_0)} &= \bar{\Phi}^{il}_{(t_2,t_1)}\bar{\Phi}^{lj}_{(t_1,t_0)} \\ \Psi^{ijk}_{(t_2,t_0)} &= \bar{\Phi}^{il}_{(t_2,t_1)}\Psi^{ljk}_{(t_1,t_0)} + \Psi^{imn}_{(t_2,t_1)}\bar{\Phi}^{mj}_{(t_1,t_0)}\bar{\Phi}^{nk}_{(t_1,t_0)}\end{aligned} \tag{33}$$

It is reasonable to assume that the initial relative state uncertainty $p(d\boldsymbol{x}_0, t_0)$ and the impulsive maneuver uncertainty $p(d\boldsymbol{x}_{v1}, t_1)$ are independent random variables. Therefore, all the cross moments, such as $E[d\boldsymbol{x}_0 d\boldsymbol{x}_{v1}]$, $E[d\boldsymbol{x}_0 d\boldsymbol{x}_0 d\boldsymbol{x}_{v1}]$, $E[d\boldsymbol{x}_0 d\boldsymbol{x}_{v1} d\boldsymbol{x}_{v1}]$, $E[d\boldsymbol{x}_0 d\boldsymbol{x}_0 d\boldsymbol{x}_0 d\boldsymbol{x}_{v1}]$, $E[d\boldsymbol{x}_0 d\boldsymbol{x}_0 d\boldsymbol{x}_{v1} d\boldsymbol{x}_{v1}]$ and $E[d\boldsymbol{x}_0 d\boldsymbol{x}_{v1} d\boldsymbol{x}_{v1} d\boldsymbol{x}_{v1}]$, are zeros. In order to propagate both the initial relative state uncertainty and the first impulsive maneuver uncertainty, substituting Eqs. (31) and (32) into Eq. (6) and considering that the cross moments are zeros, then the mean and covariance matrix of $d\boldsymbol{x}_2$ can be obtained as

$$\left[\boldsymbol{m}_2, \boldsymbol{C}_2\right] = STT\left[\boldsymbol{m}_0, \boldsymbol{C}_0; \hat{\boldsymbol{e}}_0, \delta\hat{\boldsymbol{x}}_0, \bar{\boldsymbol{\Phi}}_{(t_f,t_0)}, \boldsymbol{\Psi}_{(t_f,t_0)}\right] + STT\left[\boldsymbol{m}_{v1}, \boldsymbol{C}_{v1}; \hat{\boldsymbol{e}}_1, \delta\hat{\boldsymbol{x}}_1^+, \bar{\boldsymbol{\Phi}}_{(t_2,t_1)}, \boldsymbol{\Psi}_{(t_2,t_1)}\right] \tag{34}$$

where the similar denotation of Eq. (27) is applied to describe the propagation of impulsive maneuver uncertainty, and $\delta\hat{\boldsymbol{x}}_1^+$ is the nominal relative state after $\Delta\boldsymbol{v}_1$. $\boldsymbol{m}_{v1}$ and $\boldsymbol{C}_{v1}$ is the same with those in (29). Assuming that the impulse uncertainty $p(d\boldsymbol{x}_{v1}, t_1)$ is Gaussian distribution, then the third and fourth moments of $d\boldsymbol{x}_{v1}$ can also be computed using Eq. (26).

Equation (34) shows that the initial relative state uncertainty and the impulsive maneuver uncertainty can be independently propagated and summed at the final time.

The process of deriving Eq. (34) can be recursively applied to problem with more than one impulsive maneuvers, i.e. $t_k, \Delta\boldsymbol{v}_k$ ($k = 1, 2, \ldots, K$, $t_0 \le t_1 < \ldots < t_K \le t_f$). Considering that the impulses uncertainties $p(d\boldsymbol{x}_{vk}, t_k)$ and the initial relative state uncertainty $p(d\boldsymbol{x}_0, t_0)$ are pairwise independent, then the first two moments of final relative state uncertainty can be obtained as

$$\begin{aligned}\left[\boldsymbol{m}_f, \boldsymbol{C}_f\right] &= STT\left[\boldsymbol{m}_0, \boldsymbol{C}_0; \hat{\boldsymbol{e}}_0, \delta\hat{\boldsymbol{x}}_0, \bar{\boldsymbol{\Phi}}_{(t_f,t_0)}, \boldsymbol{\Psi}_{(t_f,t_0)}\right] \\ &\quad + \sum_{k=1}^{K} STT\left[\boldsymbol{m}_{vk}, \boldsymbol{C}_{vk}; \hat{\boldsymbol{e}}_k, \delta\hat{\boldsymbol{x}}_k^+, \bar{\boldsymbol{\Phi}}_{(t_f,t_k)}, \boldsymbol{\Psi}_{(t_f,t_k)}\right]\end{aligned} \tag{35}$$

where $\hat{\boldsymbol{e}}_k$ is Chief nominal orbital element at t_k, $\delta\hat{\boldsymbol{x}}_k^+$ is the nominal relative state after impulse $\Delta\boldsymbol{v}_k$. $\hat{\boldsymbol{e}}_k$ and $\delta\hat{\boldsymbol{x}}_k^+$ are used to compute the transitive STTs $\bar{\boldsymbol{\Phi}}_{(t_f,t_k)}, \boldsymbol{\Psi}_{(t_f,t_k)}$, which can be computed by recursively using Eq. (33). For example, replacing $\bar{\boldsymbol{\Phi}}_{(t_2,t_1)}, \boldsymbol{\Psi}_{(t_2,t_1)}$ and $\bar{\boldsymbol{\Phi}}_{(t_1,t_0)}, \boldsymbol{\Psi}_{(t_1,t_0)}$ with $\bar{\boldsymbol{\Phi}}_{(t_3,t_2)}, \boldsymbol{\Psi}_{(t_3,t_2)}$ and $\bar{\boldsymbol{\Phi}}_{(t_2,t_0)}, \boldsymbol{\Psi}_{(t_2,t_0)}$, respectively; then the STTs $\bar{\boldsymbol{\Phi}}_{(t_3,t_0)}, \boldsymbol{\Psi}_{(t_3,t_0)}$ can be computed using

Eq. (33).

As shown in Eq. (35), the first two moments of the initial relative state uncertainty and impulses uncertainties can be independently propagated and summed at the final time, this is benefitted from the fact that those input uncertainties are independent random variables and thus their cross-moments are zeros. However, as shown in Eqs. (31) and (32), the initial relative state difference $d\boldsymbol{x}_0$ and the impulse difference $d\boldsymbol{x}_{vk}$ can not be independently propagated and summed at the final time, because the cross term *dC* in Eq. (32) is non-zero.

As shown in Eq. (35), the nominal relative state $\delta\hat{\boldsymbol{x}}_k^+$ is required at each maneuver $t_k, \Delta\boldsymbol{v}_k$, it can be segmentally propagated using

$$\begin{aligned} &\delta\hat{\boldsymbol{x}}_k^+ = \delta\hat{\boldsymbol{x}}_k + \hat{\boldsymbol{x}}_{vk}, \quad \hat{\boldsymbol{x}}_{vk} = [\boldsymbol{0}_3, \Delta\hat{\boldsymbol{v}}_k]^T, \quad k = 0,1...K \\ &\delta\hat{\boldsymbol{x}}_{k+1} = \boldsymbol{\Phi}(t_{k+1}, t_k)\delta\hat{\boldsymbol{x}}_k^+ + \frac{1}{2}\boldsymbol{\Psi}(t_{k+1}, t_k) \otimes \delta\hat{\boldsymbol{x}}_k^+ \otimes \delta\hat{\boldsymbol{x}}_k^+ \end{aligned} \tag{36}$$

where $\delta\hat{\boldsymbol{x}}_0^+ = \delta\hat{\boldsymbol{x}}_0$ and $t_{K+1} = t_f$, it is noted that the STM $\boldsymbol{\Phi}(t_{k+1}, t_k)$ (but not $\hat{\boldsymbol{\Phi}}(t_{k+1}, t_k)$) is used for propagating the nominal relative state.

C. Covariance Propagation with Chief Maneuvering

The problem considering maneuvers on Chief is different from that on Deputy, because the LVLH frame used to describe the relative state is attached on Chief, thus the description of Deputy's relative state will be affected by Chief maneuvers.

Let's consider that Chief performs *K* impulsive maneuvers $t_k, \Delta\boldsymbol{v}_k$ (k = 1, 2, …, K, $t_0 \le t_1 < \ldots < t_K \le t_f$) during the propagation period $[t_0, t_f]$, then the relative trajectory is divided into (K+1) segments by *K* impulses. Denoting the real impulse as $\Delta\boldsymbol{v}_k = \Delta\hat{\boldsymbol{v}}_k + d\boldsymbol{v}_k$, the post-maneuver nominal relative state $\delta\hat{\boldsymbol{x}}_k^+$ and the post-maneuver relative state difference $d\boldsymbol{x}_k^+$ can be expressed as

$$\begin{aligned} &\delta\hat{\boldsymbol{x}}_k^+ = \boldsymbol{M}_k\left(\delta\hat{\boldsymbol{x}}_k - \hat{\boldsymbol{x}}_{vk}\right), \quad \hat{\boldsymbol{x}}_{vk} = [\boldsymbol{0}_3, \Delta\hat{\boldsymbol{v}}_k]^T \\ &d\boldsymbol{x}_k^+ = \boldsymbol{M}_k\left(d\boldsymbol{x}_k - d\boldsymbol{x}_{vk}\right), \quad d\boldsymbol{x}_{vk} = [\boldsymbol{0}_3, d\boldsymbol{v}_k]^T \end{aligned} \tag{37}$$

where k = 1, 2, …, K, $d\boldsymbol{x}_k$ is the relative state difference at t_k; $\boldsymbol{M}_k = \boldsymbol{M}_I^+(t_k)\boldsymbol{M}_L(t_k)$, $\boldsymbol{M}_L(t_k)$ is a 6×6 matrix that transform a state (position and velocity) from the Chief LVLH frame to the ICS frame, and $\boldsymbol{M}_I(t_k)$ is a state transformation matrix from the ICS frame to the Chief LVLH frame. It is noticed that, $\boldsymbol{M}_I^+(t_k) \neq [\boldsymbol{M}_L(t_k)]^{-1}$, because $\boldsymbol{M}_I^+(t_k)$ is computed based on Chief post-maneuver state at t_k. The mathematic expression of $\boldsymbol{M}_L$ and $\boldsymbol{M}_I$ were given in [41].

In order to propagate the initial relative state uncertainty and Chief's impulses uncertainties, we first consider only one impulsive maneuver $t_1, \Delta\boldsymbol{v}_1$ on Chief, and the final time is set to be t_2.

That is to propagate the initial relative state difference $d\boldsymbol{x}(t_0)$ from t_0 to t_2, during which Chief executes an impulse at t_1. Substituting Eq. (37) into Eq. (31), the relative state difference at t_2 was obtained as

$$\begin{aligned} d\boldsymbol{x}_2 &= \boldsymbol{\varphi}_{(t_2,t_1)}\left(d\boldsymbol{x}_1 - d\boldsymbol{x}_{v1}\right) + \frac{1}{2}\boldsymbol{\psi}_{(t_2,t_1)} \otimes \left(d\boldsymbol{x}_1 - d\boldsymbol{x}_{v1}\right) \otimes \left(d\boldsymbol{x}_1 - d\boldsymbol{x}_{v1}\right) \\ \boldsymbol{\varphi}_{(t_2,t_1)} &= \widehat{\boldsymbol{\Phi}}_{(t_2,t_1)}\boldsymbol{M}_1, \quad \psi^{ijk}_{(t_2,t_1)} = \Psi^{imn}_{(t_2,t_1)} M_1^{mj} M_1^{nk} \end{aligned} \tag{38}$$

By substituting Eq. (30) into Eq. (38) and comprising linear and quadratic terms only, we eliminate $d\boldsymbol{x}_1$ from the expression of $d\boldsymbol{x}_2$ and obtain

$$\begin{aligned} d\boldsymbol{x}_2 = {} & \boldsymbol{\varphi}_{(t_2,t_0)} d\boldsymbol{x}_0 + \frac{1}{2}\boldsymbol{\psi}_{(t_2,t_0)} \otimes d\boldsymbol{x}_0 \otimes d\boldsymbol{x}_0 \\ & - \boldsymbol{\varphi}_{(t_2,t_1)} d\boldsymbol{x}_{v1} + \frac{1}{2}\boldsymbol{\psi}_{(t_2,t_1)} \otimes d\boldsymbol{x}_{v1} \otimes d\boldsymbol{x}_{v1} - \boldsymbol{\varphi}_{(t_1,t_0)} \otimes \boldsymbol{\psi}_{(t_2,t_1)} \otimes d\boldsymbol{x}_0 \otimes d\boldsymbol{x}_{v1} \end{aligned} \tag{39}$$

where. $\boldsymbol{\varphi}_{(t_2,t_0)}$ and $\boldsymbol{\psi}_{(t_2,t_0)}$ are the transitive STTs from t_0 to t_2, they are calculated as below,

$$\begin{aligned} \varphi^{ij}{}_{(t_2,t_0)} &= \varphi^{il}{}_{(t_2,t_1)} \varphi^{lj}{}_{(t_1,t_0)} \\ \psi^{ijk}{}_{(t_2,t_0)} &= \varphi^{il}{}_{(t_2,t_1)} \psi^{ljk}{}_{(t_1,t_0)} + \psi^{imn}{}_{(t_2,t_1)} \varphi^{mj}{}_{(t_1,t_0)} \varphi^{nk}{}_{(t_1,t_0)} \end{aligned} \tag{40}$$

Similarly with the derivation of Eq. (35), considering the fact that the impulses uncertainties $p(d\boldsymbol{x}_{vk}, t_k)$ and the initial relative state uncertainty $p(d\boldsymbol{x}_0, t_0)$ are independent random variables, we substitute Eq. (39) into Eq. (6) and extend it to the problem with multiple impulses executing on Chief, then the mean and covariance matrix of final relative state uncertainty can be derived as

$$\begin{aligned} \left[\boldsymbol{m}_f, \boldsymbol{C}_f\right] = {} & STT\left[\boldsymbol{m}_0, \boldsymbol{C}_0; \hat{\boldsymbol{e}}_0, \delta\hat{\boldsymbol{x}}_0, \boldsymbol{\varphi}_{(t_f,t_0)}, \boldsymbol{\psi}_{(t_f,t_0)}\right] \\ & + \sum_{k=1}^{K} STT\left[\boldsymbol{m}_{vk}, \boldsymbol{C}_{vk}; \hat{\boldsymbol{e}}_k^+, \delta\hat{\boldsymbol{x}}_k^+, -\boldsymbol{\varphi}_{(t_f,t_k)}, \boldsymbol{\psi}_{(t_f,t_k)}\right] \end{aligned} \tag{41}$$

where $\hat{\boldsymbol{e}}_k^+$ is Chief nominal orbital element after the impulse $\Delta\boldsymbol{v}_k$, and $\delta\hat{\boldsymbol{x}}_k^+$ is the post-maneuver nominal relative state, which can be computed using Eq. (36) by replacing $\delta\hat{\boldsymbol{x}}_k^+ = \delta\hat{\boldsymbol{x}}_k + \hat{\boldsymbol{x}}_{vk}$ with $\delta\hat{\boldsymbol{x}}_k^+ = \boldsymbol{M}_k\left(\delta\hat{\boldsymbol{x}}_k - \hat{\boldsymbol{x}}_{vk}\right)$.

It should be noted that, in comparison to Eq. (36), there are two differences in Eq. (41). First, Chief post-maneuver orbital element $\hat{\boldsymbol{e}}_k^+$ is used; Second, there is a minus "-" before the first-order STT $\boldsymbol{\varphi}_{(t_f,t_k)}$. The relative state uncertainty can also be segmentally propagated to the final time using Eq. (29) by replacing $\widehat{\boldsymbol{\Phi}}_{(t_{k+1},t_k)}$ and $\boldsymbol{\Psi}_{(t_{k+1},t_k)}$ with $-\boldsymbol{\varphi}_{(t_{k+1},t_k)}$ and $\boldsymbol{\psi}_{(t_{k+1},t_k)}$.

Finally, let's consider the problem that both Deputy and Chief have executed impulsive maneuvers during the period $[t_0, t_f]$. This problem has two situations: 1) the maneuver time of Deputy is different from that of Chief, and 2) Deputy and Chief independently execute a maneuver at the same

time.

For the first situation, the final mean and covariance matrix can be computed by independently applying the second terms of Eqs. (36) and (41) at Deputy maneuver time and Chief maneuver time, respectively.

For the second situation, Eq. (41) can be used to compute the final mean and covariance matrix, in which the terms $\delta\hat{\boldsymbol{x}}_k^+$, $\boldsymbol{m}_{vk}$ and $\boldsymbol{C}_{vk}$ should be replaced using

$$\begin{aligned} \delta\hat{\boldsymbol{x}}_k^+ &= \boldsymbol{M}_k\left(\delta\hat{\boldsymbol{x}}_k + \hat{\boldsymbol{x}}_{vk}^D - \hat{\boldsymbol{x}}_{vk}^C\right) \\ \boldsymbol{m}_{vk} &= \boldsymbol{m}_{vk}^C - \boldsymbol{m}_{vk}^D, \quad \boldsymbol{C}_{vk} = \boldsymbol{C}_{vk}^C + \boldsymbol{C}_{vk}^D \end{aligned} \tag{42}$$

where the superscripts "*C*" and "*D*" denote Chief and Deputy, respectively. Combing Eq. (42) with (41), the first two moments of final relative state uncertainty can be propagated for the scenario with Deputy and Chief executing maneuvers simultaneously.

V. Nonlinear Propagation of Probability Density Function

Equations (27), (35) and (41) can be used to propagate the first two moments of relative state uncertainty. However, the final relative state uncertainty may not keep Gaussian distribution even though all the input uncertainties are assumed Gaussian distributions, because the Gaussian structure cannot be preserved after a nonlinear mapping such as the orbital dynamics in Eq. (4). For a non-Gaussian distribution, the first two moments are insufficient to fully describe its statistical properties. To address this problem, a method to propagate the non-Gaussian PDF is developed by combing the nonlinear covariance propagation with a GMM approach.

A. Gaussian Mixture Model

The main idea of GMM approach is to approximate an arbitrary PDF using a finite sum of weighted Gaussian density functions, i.e.,

$$\hat{p}\left(t,\boldsymbol{x}\right) = \sum_{i=1}^{N} \boldsymbol{\omega}_i p_g\left(\boldsymbol{x};\boldsymbol{m}_i,\boldsymbol{C}_i\right) \tag{43}$$

where *N* is the total number of Gaussian kernels, $\boldsymbol{m}_i$ and $\boldsymbol{C}_i$ represent the mean and covariance matrix of the i^{th} Gaussian density function $p_g\left(\boldsymbol{x};\boldsymbol{m}_i,\boldsymbol{C}_i\right)$, respectively; $\boldsymbol{\omega}_i$ denotes the weight of the i^{th} Gaussian kernel, it is determined by minimizing the difference between the real PDF $p\left(t,\boldsymbol{x}\right)$ and the approximated PDF $\hat{p}\left(t,\boldsymbol{x}\right)$ [30-32] under the positivity and normalization constraints, i.e,

$$\sum_{i=1}^{N} \boldsymbol{\omega}_i = 1; \quad \boldsymbol{\omega}_i \geq 0, \quad i = 1,2,...,N \tag{44}$$

Theoretically, the mixture PDF, $\hat{p}\left(t,\boldsymbol{x}\right)$, approximates to the real PDF $p\left(t,\boldsymbol{x}\right)$ by increasing

the number of mixtures, N. There are several methods available to split the initial Gaussian distribution into a GMM [30-32], this study employs the splitting method proposed by DeMars et al. [30]. This method first splits a univariate Gaussian distribution $p_g\left(x;0,1\right)$ into N homoscedastic components, i.e. $(\tilde{\omega}_i,\tilde{m}_i,\tilde{\sigma})$ (i = 1, 2, $\cdots N$); and then applies the univariate splitting parameters $(\tilde{\omega}_i,\tilde{m}_i,\tilde{\sigma})$ to the multivariate case using an eigenvalue decomposition, where $\tilde{\omega}_i$, $\tilde{m}_i$ and $\tilde{\sigma}$ are the weight, mean, and standard deviation for the i^{th} univariate Gaussian mixture, respectively. An advantage of this method is that the splitting process of univariate Gaussian is independent of the user's problem, thus it can be computed offline and saved as database. Vittaldev and Russell [32] provided a library data of splitting the univariate Gaussian distribution up to 39 components, in which the parameters $(N,\tilde{\sigma},\tilde{m}_i,\tilde{\omega}_i)$ (i = 1, 2, $\cdots N$) for different N ($\leq$ 39) are provided. To apply this database to the user's multivariate uncertainty propagation with PDF $p_g\left(\boldsymbol{x};\boldsymbol{m}_0,\boldsymbol{C}_0\right)$, a splitting direction needs be selected first. Generally, the direction with the largest nonlinearity is selected, for the orbital uncertainty propagation problem, the radial position or transverse velocity [30, 42, 43] usually has a larger nonlinearity than the other components. If the multivariate input uncertainty $p_g\left(\boldsymbol{x};\boldsymbol{m}_0,\boldsymbol{C}_0\right)$ is split along the j^{th} dimensionality of $\boldsymbol{x}$, then the mean and covariance matrix for the i^{th} Gaussian mixture can be expressed as [30]

$$\begin{cases} \omega_i = \tilde{\omega}_i, \quad \boldsymbol{m}_i = \boldsymbol{m}_0 + \sqrt{\lambda_j}\tilde{m}_i\boldsymbol{\upsilon}_j, \quad \boldsymbol{C}_i = \boldsymbol{V}\boldsymbol{\Lambda}_i\boldsymbol{V}^T \\ \boldsymbol{\Lambda}_i = \text{diag}\{\lambda_1,\lambda_2,...,\tilde{\sigma}^2\lambda_j,...,\lambda_n\}, \quad \boldsymbol{C}_0 = \boldsymbol{V}\boldsymbol{\Lambda}\boldsymbol{V}^T \end{cases} \tag{45}$$

where $\text{diag}\{\cdot\}$ denotes to construct a matrix with the given diagonal elements, $\boldsymbol{V}$ and $\boldsymbol{\Lambda}$ are the eigenvalue matrix and the eigenvector matrix of $\boldsymbol{C}_0$, respectively. λ_j is the j^{th} eigenvalue in $\boldsymbol{\Lambda}$, and $\boldsymbol{\upsilon}_j$ is the j^{th} column of $\boldsymbol{V}$.

Once the N Gaussian mixtures $(\omega_i,\boldsymbol{m}_i,\boldsymbol{C}_i)$ (i = 1, 2, $\cdots N$) are obtained using Eq. (45), the analytical covariance propagations of Eqs. (27), (35) and (41) are used to propagate $\boldsymbol{m}_i,\boldsymbol{C}_i$ from the initial time to the final time. The final non-Gaussian PDF then is computed using Eq. (43), and the final mean and covariance matrix is merged as follows [30].

$$\begin{aligned} \boldsymbol{m}_m &= \sum_{i=1}^{N}\frac{\boldsymbol{\omega}_i}{\omega_m}\boldsymbol{m}_i, \quad \omega_m = \sum_{i=1}^{N}\boldsymbol{\omega}_i \\ \boldsymbol{C}_m &= \sum_{i=1}^{N}\frac{\boldsymbol{\omega}_i}{\omega_m}\left(\boldsymbol{C}_i + \boldsymbol{m}_i\boldsymbol{m}_i^T\right) - \boldsymbol{m}_m\boldsymbol{m}_m^T \end{aligned} \tag{46}$$

The weights updating during the propagation process is not considered in this study, readers with an interest on this topic can refer to [31].

B. Method Combining GMM and STTs

For the uncertainty propagation with Deputy or Chief executing impulsive maneuvers, it needs to split the input uncertainties (including initial relative state uncertainty and impulsive maneuver uncertainties) into N Gaussian mixtures, and then to propagate every Gaussian mixture to the final time using Eqs. (27), (35) or (41).

Based on the theoretical concepts of GMM method, the propagation of PDF based on the method of combining GMM and STTs can be summarized as follows.

Step 1: Combine the initial relative state uncertainty and impulses uncertainties together as an extended, (n+3K)-dimensional state: $\boldsymbol{X} = [d\boldsymbol{x}_0, d\boldsymbol{v}_1, ..., d\boldsymbol{v}_K]$, assume that the initial relative state uncertainty and impulses uncertainties are pairwise independent, Gaussian random variables, then the mean and covariance matrix of the input uncertainty vector $\boldsymbol{X}$ can be expressed as

$$\begin{aligned} \bar{\boldsymbol{m}}(t_0) &= \left[\boldsymbol{m}(t_0), E[d\boldsymbol{v}_1], ..., E[d\boldsymbol{v}_m]\right]^T \\ \bar{\boldsymbol{C}}(t_0) &= \begin{bmatrix} \boldsymbol{C}(t_0) & \boldsymbol{0}_{6\times3} & \cdots & \boldsymbol{0}_{6\times3} \\ \boldsymbol{0}_{3\times6} & \boldsymbol{C}(d\boldsymbol{v}_1) & \boldsymbol{0}_{3\times3} & \vdots \\ \vdots & \boldsymbol{0}_{3\times3} & \ddots & \boldsymbol{0}_{3\times3} \\ \boldsymbol{0}_{3\times6} & \cdots & \boldsymbol{0}_{3\times3} & \boldsymbol{C}(d\boldsymbol{v}_m) \end{bmatrix} \end{aligned} \tag{47}$$

Step 2: Split the multivariate Gaussian distribution $p_g\left(\boldsymbol{x}; \bar{\boldsymbol{m}}(t_0), \bar{\boldsymbol{C}}(t_0)\right)$ into N Gaussian mixtures $\left(\boldsymbol{\omega}_i, \bar{\boldsymbol{m}}_i, \bar{\boldsymbol{P}}_i\right)$ (i = 1, 2, …, N) using Eq. (45) and the library data given by Vittaldev and Russell [32].

Step 3: Extract the input statistical moments, i.e. $\boldsymbol{m}_i(t_0)$, $\boldsymbol{C}_i(t_0)$, $E[d\boldsymbol{v}_k]_i$ and $\boldsymbol{C}_i(d\boldsymbol{v}_k)$ (i = 1, 2, …, N, k = 1, 2, …, K), from the split Gaussian mixtures $\left(\bar{\boldsymbol{m}}_i, \bar{\boldsymbol{P}}_i\right)$. Propagate these moments to the final time using Eqs. (27), (35) or (41), then obtain the corresponding final moments of relative state uncertainty, i.e. $\left[\boldsymbol{m}_i(t_f), \boldsymbol{C}_i(t_f)\right]$. It is noted that the transitive STTs in Eqs. (27), (35) or (41) only need to compute once for propagating all the Gaussian mixtures, because all the nonzero mean Gaussian mixtures can be nonlinearly propagated using the same STTs.

Step 4: Compute the PDF and moments of final relative state uncertainty using Eqs. (43) and (46), respectively.

By combing the STTs-based covariance propagation with the GMM method, the PDF and moments of final relative state uncertainty can be analytically computed.

VI. Simulation Results

In this section, the accuracy of the analytical methods developed in Secs. IV and V are demonstrated with numerical results. To evaluate their accuracy, we first analytically compute the first two moments and the PDF using the analytical methods, and then compare them with the distribution calculated from Monte Carlo simulations. In the simulation, Chief is located at an 800 km altitude, near-circular orbit, its initial orbital elements (semi-major axis, eccentricity, inclination, right ascension of the ascending node, argument of periapsis, and true anomaly) is: $\boldsymbol{E}_C(t_0)$ = [7181.728 km, 0.0005, 45°, 250°, 90°, 30°]. Deputy's initial nominal relative state is selected as: $\delta\hat{\boldsymbol{x}}(t_0)$ = [8.660 km, -10 km, 17.321 km, -5.187 m/s, -17.967 m/s, -10.374 m/s]. This initial relative orbit is described in Chief LVLH frame, and its projection in the *yz*-plane is a circle of radius as $r_\rho = 20$ km. Chief appears at the center of the circle, and the initial phase angle between Chief and Deputy in the *yz*-plane is $\alpha_\rho = 0$. The simulation time is half a day, corresponding to the initial time t_0 = 0 s and the final time t_f = 43200 s.

The initial relative state uncertainty is assumed as zero mean Gaussian distribution with its standard deviation being: $\boldsymbol{\sigma}_{\delta x}(t_0)$ = [50 m, 80 m, 30 m, 0.3 m/s, 0.4 m/s, 0.2 m/s]. Because the maneuver uncertainties are typically proportional to the maneuver magnitudes, the standard deviations of impulsive maneuvers are set as: $\boldsymbol{\sigma}_{\Delta v_k} = a\left|\Delta\hat{\boldsymbol{v}}_k\right| + b$ (k = 1, 2, …, K), where $|\cdot|$ denotes the absolute value, and the coefficients a = 0.002, b = 0.05. The number of MC samples is 10000, and the number of GMM mixtures is N = 21. The numerical simulations are performed on a personal computer with CPU 3.60 GHz, Intel core i7 processor.

Because different scenarios (i.e., free relative motion in Sec. VI.B, relative motion with Deputy maneuvering in Sec. VI.C, and relative motion with Chief maneuvering in Sec. VI.D) are considered, we use different acronyms to label the methods used in different scenarios, they are explained in Table 1. For the LinCov method in Table 1, it should be noted that the STM $\boldsymbol{\Phi}$ in Eq. (21) can be directly used to propagate the relative state uncertainty if only the first-order solution is considered, and that the result of transitive propagation (i.e. a first-order solution of Eq. (27)) is the same with that of segmented propagation (i.e. a first-order solution of Eq. (29)) as the STM is naturally transitive (i.e. $\boldsymbol{\Phi}_{(t_f,t_0)} = \boldsymbol{\Phi}_{(t_f,t)}\boldsymbol{\Phi}_{(t,t_0)}$).

Table 1 Explanation of the acronyms for different methods used in different scenarios

Method	Explanation
MC	Numerically integrating the dynamics of both satellites in the ECI frame using Eq. (2), transforming their states from ECI frame to Chief LVLH frame and differencing them to obtain the relative state.
LinCov	It denotes the covariance propagation using Eq. (7).
gmmSTT	It denotes the combing GMM and STTs method given in Sec. V, in which the respective tranSTT

	is used for a specific scenario corresponding to Sec. VI.B, VI.C or VI.D.
tranSTT	In Sec. VI.B and VI.D, it denotes the covariance propagation using Eq. (27). In Sec. VI.C, it denotes the covariance propagation using Eq. (35). In Sec. VI.D, it denotes the covariance propagation using Eq. (41).
segmSTT	In Sec. VI.B and VI.D, it denotes the covariance propagation using Eq. (27), however, the STM $\bar{\boldsymbol{\Phi}}$ is replaced by the $\boldsymbol{\Phi}$ in Eq. (21). In Sec. VI.C, it denotes the covariance propagation using Eq. (29). In Sec. VI.D, it denotes the covariance propagation using Eq. (29), however, the STTs $\bar{\boldsymbol{\Phi}},\boldsymbol{\Psi}$ are replaced by the STTs $-\boldsymbol{\varphi},\boldsymbol{\psi}$ in Eq. (41).

A. Accuracy Analysis of Relative State Propagation

In order to validate the accuracy of Eq. (21) on relative orbit propagation, the propagation results of different analytical solutions are compared with the numerical results. The propagation errors on relative position ($\delta r = \|\delta \boldsymbol{r}\|$) and velocity ($\delta v = \|\delta \boldsymbol{v}\|$) are shown in Figs. 1 and 2, in which "C-W" denotes the C-W equations [2], "Gim and Alfriend" denotes the linear J_2-perturbed solution in [6], "Sengupta et al." denotes the nonlinear J_2-perturbed solution in [14], and "This paper" denotes the nonlinear J_2-perturbed solution in Eq. (21). For the results of "Sengupta et al.", we use Eq. (17) instead of the Eq. (46) in [14], because we thought there might be a small typo for the Eq. (46) in [14], as explained in Sec. III.C.

As shown in Figs. 1 and 2, the accuracy of Eq. (21) is almost the same with the solution given by Sengupta et al. [14]. Nevertheless, as illustrated by the enlarged view of Fig. 1, Eq. (21) obtains a bit improvement on relative position propagation through using osculating orbital elements instead of mean orbital elements in the second-order state transition of relative motion. This study mainly focus on the propagation of relative state uncertainty by using Eq. (21), more results about relative state propagation can refer to [6, 14, 44].

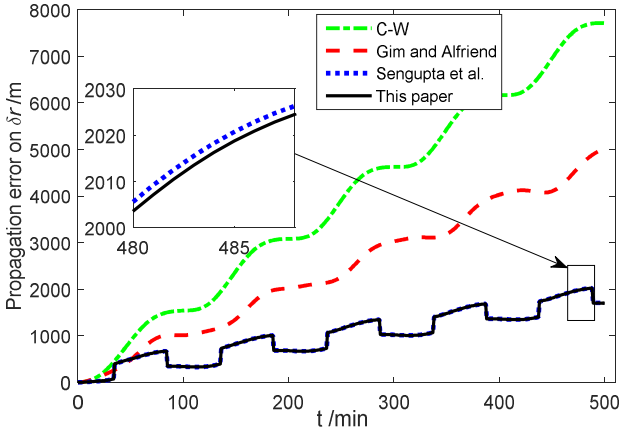

Fig. 1 Relative position propagation error

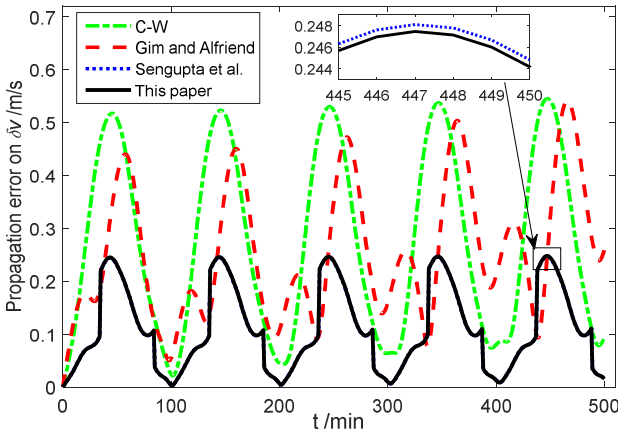

Fig. 2 Relative velocity propagation error

B. Results for Free Relative Motion

In order to validate the uncertainty propagation method developed in Sec. IV.A for the scenario of free relative motion, the initial relative state uncertainty is propagated to the final time using different methods interpreted in Table 1. The final relative state uncertainty and their 3σ ellipsoids are projected to two coordinate planes and illustrated in Figs. 3~6. The detailed absolute errors on means and standard deviations are compared in Tables 2 and 3, respectively. For the clarity of comparison, the means and standard deviations of MC simulations are presented in the second rows.

As shown in Tables 2 and 3, the errors of segmSTT method are larger than those of tranSTT method on propagating the first two moments. For example, the error of σ_y (standard deviation of transverse position) for the tranSTT is only 7.86 m, however, it is 81.18 m for the segmSTT. It means that the analytical STTs for relative motion ($\boldsymbol{\Phi}$,$\boldsymbol{\Psi}$ in Eq. (21)) cannot be directly used to propagate the relative state uncertainty unless a correction is implemented on $\boldsymbol{\Phi}$, as shown in Eq. (24). Moreover, the tranSTT method also has a better accuracy than the LinCov method as the second-order terms are considered. Almost the same accuracy is witnessed between the tranSTT and gmmSTT methods. Thus, there is no need to adopt the more complex gmmSTT method if only the first two moments are required.

The accuracies of different methods are vividly compared in Figs. 3~6. Evidently, in comparison to the segmSTT and LinCov methods, the 3σ error ellipsoids of the tranSTT provide good agreement with the results of MC simulations. As shown in Fig. 3, the final relative state uncertainty becomes non-Gaussian after a nonlinear propagation. Although the tranSTT method provides good agreements with MC simulations on propagating mean and covariance matrix, the first two moments are insufficient to fully describing the non-Gaussian distribution. Therefore, the gmmSTT method is necessary to approximate the PDF of final uncertainty which is non-Gaussian distribution. The results are presented in Figs. 7~8.

Table 2 Comparisons of final means for free relative motion

Mean	m_x (m)	m_y (m)	m_z (m)	m_{vx} (m/s)	m_{vy} (m/s)	m_{vz} (m/s)	Computation time (s)
MC	-195.48	-9.95	-0.20	-0.006	0.004	0.001	760.543
tranSTT−MC	-0.84	-0.51	0.06	0.001	0.001	-0.001	0.061
segmSTT−MC	-0.85	-0.52	0.06	0.001	0.001	-0.001	0.051
LinCov−MC	195.48	9.95	0.20	0.006	-0.004	-0.001	0.010
gmmSTT−MC	-0.68	-0.50	0.06	0.001	0.001	-0.001	0.223

Table 3 Comparisons of final standard deviations for free relative motion

Covariance	σ_x (m)	σ_y (m)	σ_z (m)	σ_{vx} (m/s)	σ_{vy} (m/s)	σ_{vz} (m/s)
MC	360.56	52460.25	237.30	0.623	0.489	0.142
tranSTT−MC	4.23	7.86	0.24	0.001	0.000	-0.004
segmSTT−MC	66.83	81.18	-85.12	0.019	-0.025	-0.011
LinCov−MC	-35.64	81.18	-85.12	0.019	-0.025	-0.011
gmmSTT−MC	3.41	-14.15	0.17	0.001	0.000	-0.004

Figure 7 gives the 3σ error ellipsoids of the 21 Gaussian mixtures propagated using the tranSTT method, as is shown, the MC samples are well surrounded by the 3σ error ellipsoids, it shows that the gmmSTT method is effective to capture the non-Gaussian uncertainty. Additionally, the PDF computed using the gmmSTT method is shown in Fig. 8, it can be seen that the PDF of gmmSTT has contours which well matches of the curvature of the MC samples.

The computation times are given in Table 2, comparing to the MC method (760.543 s), the tranSTT (0.061 s) method has comparable accuracy but much smaller computation time. Although the LinCov (0.010 s) is more efficient, it has lower accuracy than the tranSTT for nonlinear, non-Gaussian uncertainty propagation.

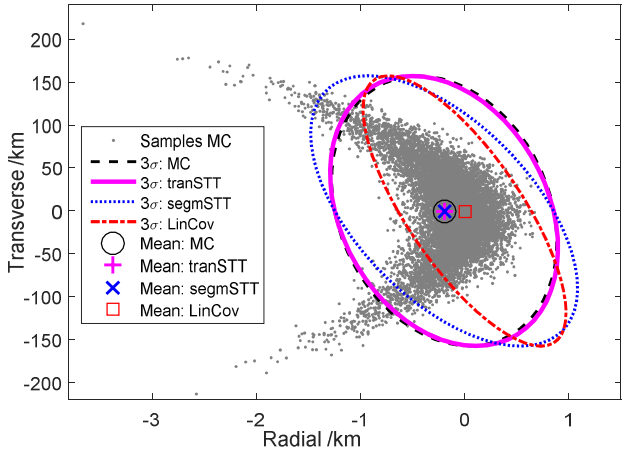

Fig. 3 *xy*-plane projection of final position uncertainty for free relative motion

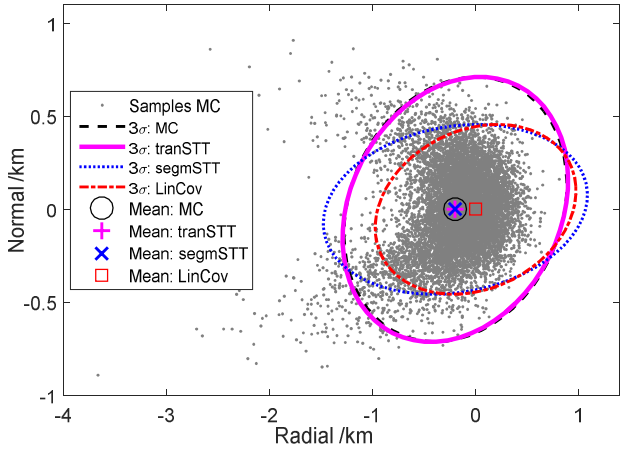

Fig. 4 *xz*-plane projection of final position uncertainty for free relative motion

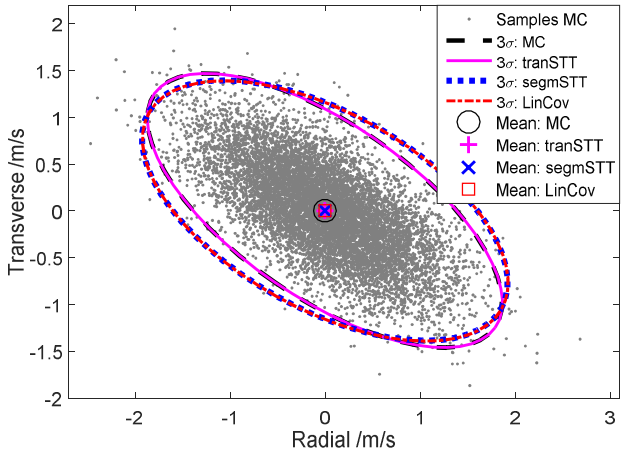

Fig. 5 $v_x v_y$-plane projection of final velocity uncertainty for free relative motion

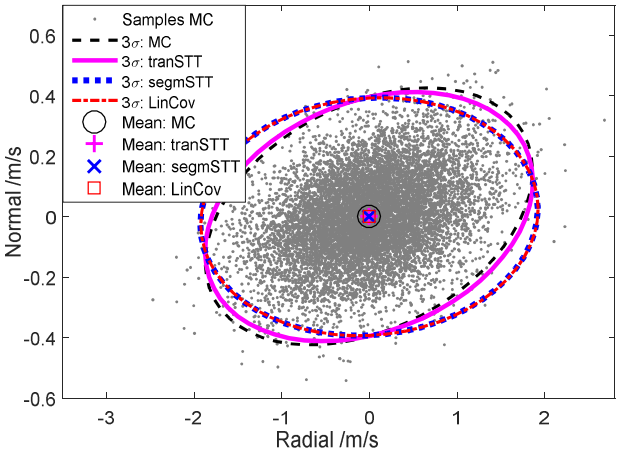

Fig. 6 $v_x v_z$-plane projection of final velocity uncertainty for free relative motion

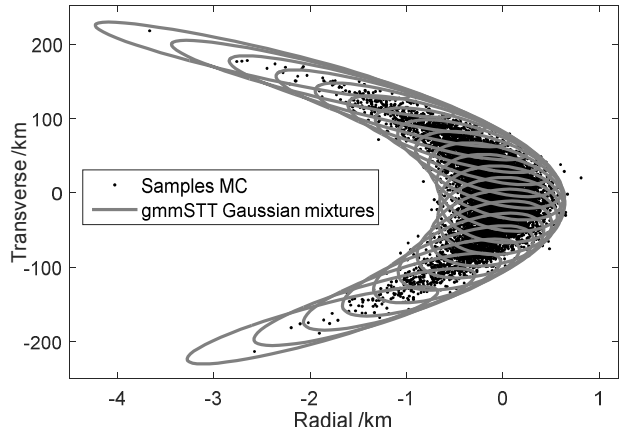

Fig. 7 xy-plane projection of Gaussian mixtures for free relative motion

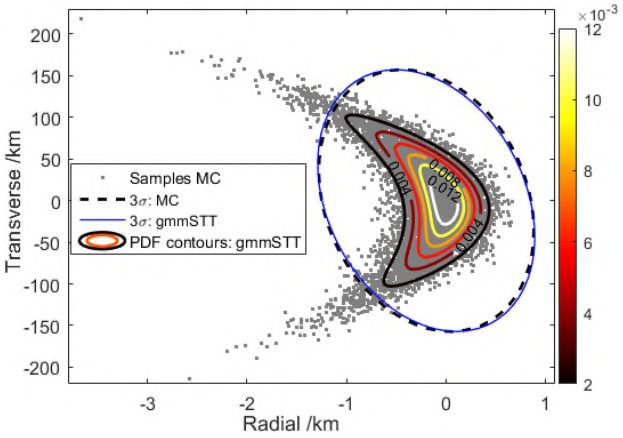

Fig. 8 xy-plane projection of PDF contours for free relative motion

C. Results for Relative Motion with Deputy Maneuvering

In order to validate the uncertainty propagation method developed in Sec. IV.B for the relative motion with Deputy maneuvering, the initial relative state uncertainty and the impulses uncertainties are propagated to the final time using different methods interpreted in Table 1. The nominal impulses are given in Table 4, these two impulses are computed using Eq. (21), they are used to reconfigure Deputy from the given initial relative state (20 km) to a final hold point ($\delta\hat{\boldsymbol{x}}(t_f)$ = [0, -5 km, 0, 0, 0, 0]) under the analytical relative motion of Eq. (21).

Table 4 Nominal impulses for relative motion with Deputy maneuvering

Impulses	t_k (s)	Δv_{kx} (m/s)	Δv_{ky} (m/s)	Δv_{kz} (m/s)
$k = 1$	22770.86	-0.104	0.818	-1.765
$k = 2$	28216.38	-9.167	-0.860	-19.291

Table 5 Comparisons of final means for relative motion with Deputy maneuvering

Mean	m_x (m)	m_y (m)	m_z (m)	m_{vx} (m/s)	m_{vy} (m/s)	m_{vz} (m/s)	Computation time (s)
MC	-182.05	-10.77	-0.20	-0.004	0.004	0.001	772.952
tranSTT−MC	-12.56	287.67	-5.96	-0.001	0.040	-0.001	0.073
segmSTT−MC	-31.20	256.56	-5.96	-0.003	0.036	-0.001	0.069
LinCov−MC	-182.05	10.77	0.20	0.004	-0.004	-0.001	0.015
gmmSTT−MC	-12.40	287.43	-5.95	-0.001	0.040	-0.001	0.442

Table 6 Comparisons of final standard deviations for relative motion with Deputy maneuvering

Covariance	σ_x (m)	σ_y (m)	σ_z (m)	σ_{vx} (m/s)	σ_{vy} (m/s)	σ_{vz} (m/s)
MC	432.21	50560.40	206.29	0.646	0.651	0.167
tranSTT−MC	14.54	319.93	2.99	0.008	0.000	-0.002
segmSTT−MC	599.75	3828.15	4.13	0.061	1.462	-0.002
LinCov−MC	-15.10	2067.13	-49.12	0.005	0.012	-0.004
gmmSTT−MC	13.89	298.67	2.94	0.007	0.000	-0.002

The final relative position uncertainty and their 3σ ellipsoids are projected to two coordinate planes and illustrated in Figs. 9~10. The detailed absolute errors of means and standard deviations are compared in Tables 5 and 6, respectively. As shown in Table 6, the tranSTT method is more accurate than the segmSTT and LinCov methods on standard deviations.

However, as shown in Table 5, the tranSTT method mismatches MC simulations on the means of transverse position and velocity, and its accuracy on propagation means even worse than LinCov method. The reason may be that only the average effects of J_2-perturbation are considered in Eq. (21). In fact, the mean error of 287.67 m on the transverse relative position is relatively small compared to its standard deviation (50560.4 m). In contrast, an evident improvement on radial component has been obtained comparing the tranSTT with the LinCov. As shown in Figs. 9 and 10, compared to the segmSTT and LinCov method, the 3σ error ellipsoids of tranSTT are obviously well matched with the MC simulation. That is, the tranSTT method still has better accuracy than the segmSTT and LinCov methods on propagation the first two moments for the scenario with Deputy maneuvering.

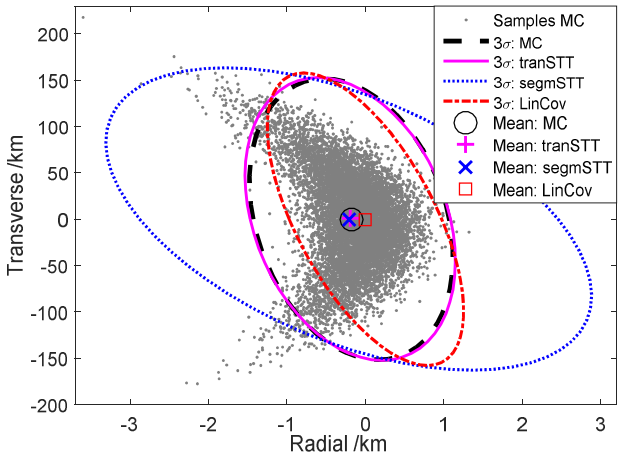

Fig. 9 *xy*-plane projection of final position uncertainty for relative motion with Deputy maneuvering

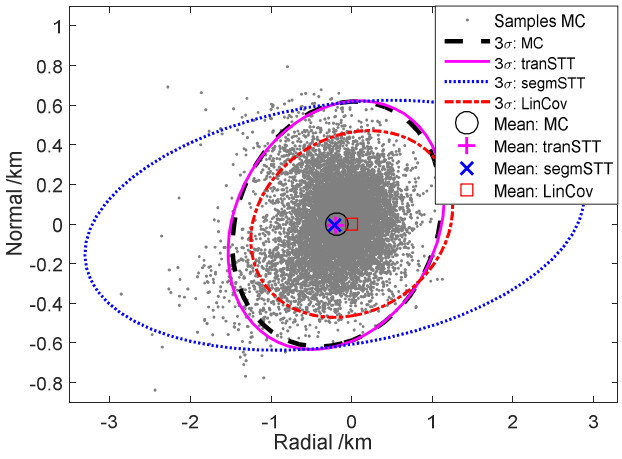

Fig. 10 *xz*-plane projection of final position uncertainty for relative motion with Deputy maneuvering

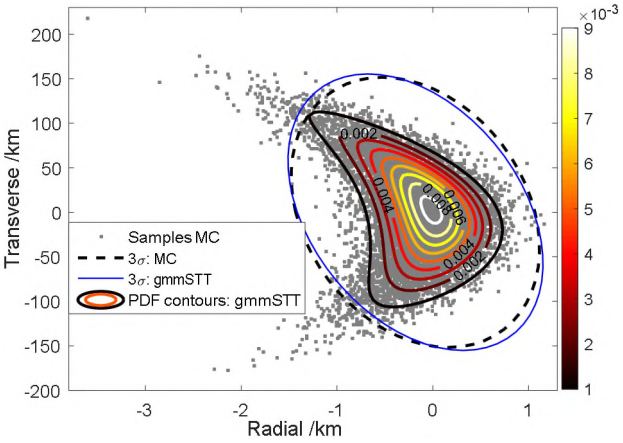

Fig. 11 *xy*-plane projection of PDF contours for relative motion with Deputy maneuvering

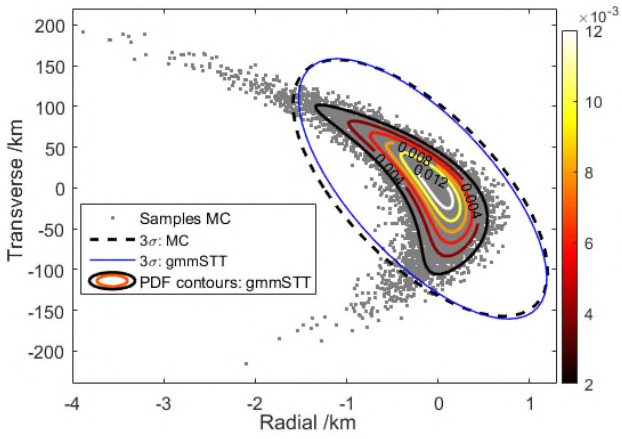

Fig. 12 *xy*-plane projection of PDF contours for relative motion with Chief maneuvering

As shown in Tables 5 and 6, the gmmSTT method still witnesses the similar accuracy with the tranSTT method on propagating the first two moments. Moreover, as shown in Fig. 11, the PDF of gmmSTT has contours which well matches of the curvature of the MC samples, it demonstrates that the gmmSTT method is effective to capture the non-Gaussian distribution for this scenario with Deputy maneuvering.

D. Results for Relative Motion with Chief Maneuvering

In order to validate the uncertainty propagation method developed in Sec. IV.C for the relative motion with Chief maneuvering, the initial relative state uncertainty and impulses uncertainties are propagated to the final time using different methods interpreted in Table 1. The nominal impulses are given in Table 7, these two impulses are computed using Eq. (21), they are used to maneuver Chief so that the relative state of Deputy can be reconfigured from the given initial value (20 km) to a final hold point ($\delta\hat{\boldsymbol{x}}(t_f)$ = [0, -5 km, 0, 0, 0, 0]) under the analytical relative motion of Eq. (21).

The final relative position uncertainty and their 3σ ellipsoids are projected to two coordinate planes and illustrated in Figs. 13~14. The detailed absolute errors on means and standard deviations are compared in Tables 8 and 9, respectively.

Table 7 Nominal impulses for relative motion with Chief maneuvering

Impulses	t_k (s)	Δv_{kx} (m/s)	Δv_{ky} (m/s)	Δv_{kz} (m/s)
$k = 1$	31566.21	-2.494	1.468	-4.74
$k = 2$	37266.69	-6.821	-1.375	-16.252

Table 8 Comparisons of final means for relative motion with Chief maneuvering

Mean	m_x (m)	m_y (m)	m_z (m)	m_{vx} (m/s)	m_{vy} (m/s)	m_{vz} (m/s)	Computation time (s)
MC	-195.71	-10.66	-0.12	-0.006	0.004	0.001	853.201
tranSTT−MC	26.77	-995.25	-7.39	-0.011	0.000	-0.002	0.083
segmSTT−MC	11.13	-1034.49	-7.37	-0.012	-0.001	-0.002	0.075
LinCov−MC	195.71	10.66	0.12	0.006	-0.004	-0.001	0.019
gmmSTT−MC	26.91	-994.41	-7.38	-0.011	0.000	-0.002	0.606

Table 9 Comparison of final standard deviations for relative motion with Chief maneuvering

Covariance	σ_x (m)	σ_y (m)	σ_z (m)	σ_{vx} (m/s)	σ_{vy} (m/s)	σ_{vz} (m/s)
MC	463.99	52441.06	154.70	0.665	0.492	0.166
tranSTT−MC	-11.31	785.92	-1.81	-0.013	0.002	-0.001
segmSTT−MC	27.38	3420.16	-1.18	0.030	0.030	-0.003
LinCov−MC	-131.32	-1174.39	11.05	0.007	-0.023	-0.001
gmmSTT−MC	-11.87	763.48	-1.82	-0.013	0.002	-0.002

For this scenario (relative motion with Chief maneuvering), the accuracies and computation times on propagating the first two moments for different methods show similar trends with those in Sec. VI.C (the scenario with Deputy maneuvering). Therefore, we do not discuss the accuracy comparison results in detail again in this section. Based on the results presented in Tables 8~9 and Figs 13~14, it is found that, for this scenario, the tranSTT method is still more accurate than the segmSTT and LinCov methods on propagating the first two moments.

Additionally, the results of the gmmSTT are compared with MC simulations in Fig. 12, as is shown, the PDF contours of gmmSTT well match the curvature of the MC samples, it demonstrates that the gmmSTT method is still effective to capture the final non-Gaussian distribution for this scenario.

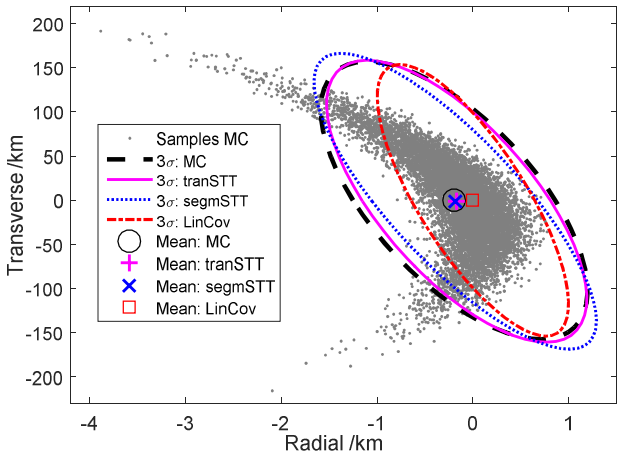

Fig. 13 *xy*-plane projection of final position uncertainty for relative motion with Chief maneuvering

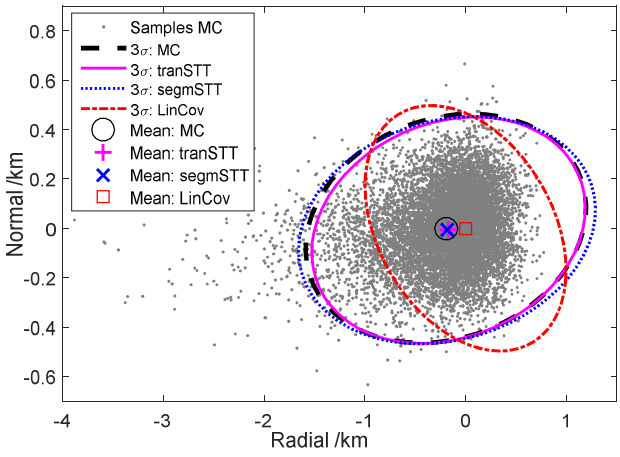

Fig. 14 *xz*-plane projection of final position uncertainty for relative motion with Chief maneuvering

E. Propagation Errors under Different Initial Conditions

In sections VI.B~VI.D, the initial relative orbit size is fixed as $r_\rho = 20$ km, and the uncertainty propagation time is fixed as $t_f = 0.5$ day. In order to validate the accuracy of the proposed method, the analytical methods are compared with the numerical MC simulation under different initial conditions, i.e., different initial relative-orbit sizes (r_ρ from 10 km to 55 km) and different propagation times (t_f from 0.5 day to 5 days). The other input parameters are kept the same with the scenario of free relative motion (Sec. VI.B). For this purpose, the following root mean square error (RMSE) in the stand deviations are computed as

$$e_r = \sqrt{\frac{1}{3}\sum_{i=x,y,z}\left[\sigma_i(t_f)-\sigma_i^{\mathrm{MC}}(t_f)\right]^2} \tag{48}$$

$$e_v = \sqrt{\frac{1}{3}\sum_{i=vx,vy,vz}\left[\sigma_i(t_f)-\sigma_i^{\mathrm{MC}}(t_f)\right]^2} \tag{49}$$

where e_r and e_v are the position and velocity RMSE, respectively, σ_i and σ_i^{MC} are the standard deviation of final relative state uncertainty respectively computed using the proposed analytical method and the MC simulation.

The position and velocity RMSE for different methods are compared in Fig. 15 ($t_f = 0.5$ day) and Fig. 16 ($r_\rho = 20$ km). Obviously, the RMSE diverge more quickly with the propagation time (Fig. 16) than with the relative-orbit sizes (Fig. 15). As shown in Fig. 15, with the increasing of relative-orbit size (r_ρ from 10 km to 55 km), the RMSE of segmSTT and LinCov methods diverge quickly, while the RMSE of tranSTT and gmmSTT methods diverge much slowly. Since the second-order nonlinear terms are correctly included in tranSTT and gmmSTT methods, their RMSE are

small (less than 800 m) even though the initial relative-orbit size reaches 55 km. As shown in Fig. 6, for different propagation time, the tranSTT and gmmSTT methods still witness better accuracies than segmSTT and LinCov methods, their position RMSE are less than 2.5 km even for 5-day propagation. Additionally, as the tranSTT and gmmSTT methods are analytical, their computation times remain unchanged (almost the same with those in Table 2) for both Figs. 15 and 16. However, for the 5-day propagation in Fig. 16, the MC simulation requires more than 7600 s of computation time.

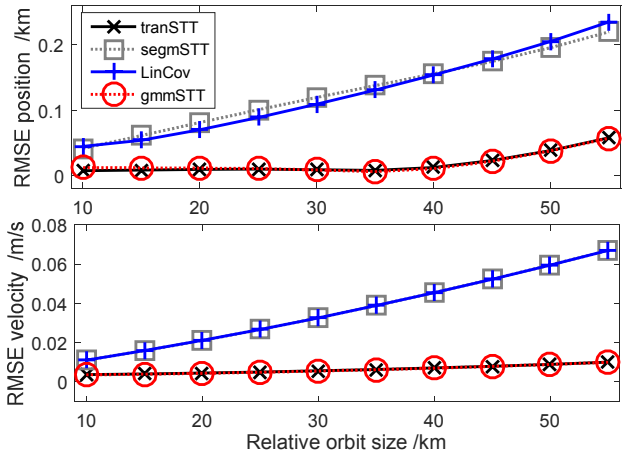

Fig. 15 position and velocity RMSE under different initial relative-orbit sizes

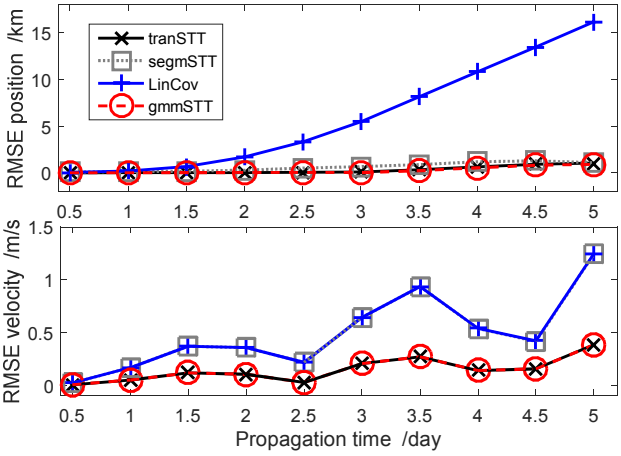

Fig. 16 position and velocity RMSE under different propagation time

F. Summary and Discussion

In summary, based on the results and analysis presented in Secs. VI.B~VI.E, the STTs-based uncertainty propagators (tranSTT and gmmSTT) developed in this study not only provide good accuracy matching of MC simulations but also are computationally efficient.

(1) As shown in Sec. VI.B, the previously proposed STTs (Eq. (21)) that used for relative state propagation cannot be directly employed to propagate relative state uncertainty. Instead, the revised STTs (Eq. (24)) given in this study can be used, and it has better accuracy than the previous ones.

(2) As shown in Secs. VI.C and VI.D, for relative state uncertainty propagation with abrupt state jumps (e.g. Deputy or Chief executes maneuvers), the transitive STTs (Eqs. (35) and (41)) derived in this paper has better accuracy than the segmented STTs (Eq. (29)) on relative state uncertainty propagation. Because the truncation error will be increasingly enlarged by the segmented STTs with the statistical moments being dispersed by the segmented trajectories one after another.

(3) As shown in Sec. VI.E, as the second-order nonlinear terms are correctly included in the proposed methods (tranSTT and gmmSTT), the proposed methods are suitable for problems with large initial relative-orbit size r_ρ or long propagation time t_f. The defined RMSE of standard deviation is less than 800 m for r_ρ up to 55 km, and this RMSE is less than 3 km for t_f up to 5 days.

(4) The proposed methods (tranSTT and gmmSTT) are analytical, and thus they are computationally much more efficient than MC simulation. The computation times for all scenarios, as shown in Tables 2, 5 and 8, are less than 1 second, which is less than 0.2% of the computation time for MC simulation. It is potentially suitable for satellite onboard computation.

(5) The known shortcomings of the proposed methods are: First, the STTs are singular for zero inclination orbits ($i \approx 0$ deg); Second, the expressions for computing the STTs are relatively complex. However, the concepts of accounting for the second-order nonlinear terms and the abrupt state jumps on relative state uncertainty propagation can be used to extend the current method through combing it with the state-of-art analytical STTs in relative motion (e.g., [8, 9, 12]).

VII. Conclusions

An analytical uncertainty propagation method based on state transition tensors (STTs) is developed for satellite relative motion near J_2-perturbed, elliptic orbits. First, the second-order STTs for propagating the relative state difference are derived based on the nonlinear analytical solution for relative motion, these STTs are obtained by adding a correction into the first-order solution of relative state. Second, based on the STTs for free relative motion, a new set of transitive STTs is derived to propagate uncertainties for relative motion with abrupt state jumps, e.g. impulsive maneuvers executing on the two satellites (denotes as Deputy and Chief). Third, the nonlinear covariance propagation is formulated by combining the STTs with the covariance analysis method. Finally, the nonlinear propagation of the probability density function (PDF) has been constructed by combining the STTs with a Gaussian mixture model.

Different scenarios, i.e. free relative motion, relative motion with Deputy maneuvering, and relative motion with Chief maneuvering, have been used to validate the proposed STTs-based uncertainty propagator. Numerical results show that the proposed method provides good agreement with Monte Carlo simulations on covariance and PDF propagations, and that the proposed method outperforms the traditional linear covariance method since the second-order terms are taken into account. Additionally, as the STTs can be analytically computed, and the splitting of univariate Gaussian distribution can be done offline, the proposed uncertainty propagation method can be computationally efficient.

Acknowledgements

The authors acknowledge financial support from the National Natural Science Foundation of China (No. 11572345, 11402295 and 11222215), the 973 Project (No. 2013CB733100).

References

[1] Alfriend, K., Vadali, S. R., Gurfil, P., How, J., and Breger, L. *Spacecraft formation flying: Dynamics, control and navigation*. Oxford, UK: Butterworth-Heinemann, Elsevier, 2010.

[2] Clohessy, W. H., and Wiltshire, R. S. "Terminal guidance system for satellite rendezvous," *Journal of the Aerospace Sciences*, Vol. 27, No. 9, 1960, pp. 653-658.

[3] Tschauner, J., and Hempel, P. "Rendezvous zu Einem in Elliptischer Bahn um Laufenden Ziel," *Astronautica Acta*, Vol. 11, No. 5, 1965, pp. 312-321.

[4] Schweighart, S. A., and Sedwick, R. J. "High-fidelity linearized J model for satellite formation flight," *Journal of Guidance, Control, and Dynamics*, Vol. 25, No. 6, 2002, pp. 1073-1080.

[5] Yamanaka, K., and Ankersen, F. "New State Transition Matrix for Relative Motion on an Arbitrary Elliptical Orbit," *Journal of Guidance, Control, and Dynamics*, Vol. 25, No. 1, 2002, pp. 60-66.
doi: 10.2514/2.4875

[6] Gim, D.-W., and Alfriend, K. T. "State Transition Matrix of Relative Motion for the Perturbed Noncircular Reference Orbit," *Journal of Guidance, Control, and Dynamics*, Vol. 26, No. 6, 2003, pp. 956-971.
doi: 10.2514/2.6924

[7] Gim, D.-W., and Alfriend, K. T. "Satellite Relative Motion Using Differential Equinoctial Elements," *Celestial Mechanics and Dynamical Astronomy*, Vol. 92, No. 4, 2005, pp. 295-336.
doi: 10.1007/s10569-004-1799-0

[8] Mahajan, B., Vadali, S. R., and Alfriend, K. T. "Analytic Solution for the Satellite Relative Motion: The Complete Zonal Gravitational Problem," *Proceedings of the 26th AAS/AIAA Space Flight Mechanics Meeting*. Univelt, Napa, CA, 2016.

[9] Koenig, A. W., Guffanti, T., and D'Amico, S. "New State Transition Matrices for Spacecraft Relative Motion in Perturbed Orbits," *Journal of Guidance, Control, and Dynamics*, 2017, pp. 1-20.
doi: 10.2514/1.G002409

[10] Schaub, H. "Relative Orbit Geometry Through Classical Orbit Element Differences," *Journal of Guidance, Control, and Dynamics*, Vol. 27, No. 5, 2004, pp. 839-848.
doi: 10.2514/1.12595

[11] Bennett, T., and Schaub, H. "Continuous-Time Modeling and Control Using Nonsingular Linearized Relative-Orbit Elements," *Journal of Guidance, Control, and Dynamics*, Vol. 39, No. 12, 2016, pp. 2605-2614.
doi: 10.2514/1.g000366

[12] Biria , A. D., and Russell, R. P. "A Satellite Relative Motion Model Including J2 and J3 via Vinti's Intermediary," *Advances in the Astronautical Sciences* Vol. 158, 2016.

[13] Gurfil, P., and Kasdin, N. J. "Nonlinear Modelling of Spacecraft Relative Motion in the Configuration Space," *Journal of Guidance, Control, and Dynamics*, Vol. 27, No. 1, 2004, pp. 154-157.
doi: 10.2514/1.9343

[14] Sengupta, P., Vadali, S. R., and Alfriend, K. T. "Second-order state transition for relative motion near perturbed, elliptic orbits," *Celestial Mechanics and Dynamical Astronomy*, Vol. 97, No. 2, 2007, pp. 101-129.
doi: 10.1007/s10569-006-9054-5

[15] Sullivan, J., Grimberg, S., and D'Amico, S. "Comprehensive Survey and Assessment of Spacecraft Relative Motion Dynamics Models," *Journal of Guidance, Control, and Dynamics*, 2017, pp. 1-23.
doi: 10.2514/1.g002309

[16] Lee, S., Lyu, H., and Hwang, I. "Analytical Uncertainty Propagation for Satellite Relative Motion Along Elliptic Orbits," *Journal of Guidance, Control, and Dynamics*, Vol. 39, No. 7, 2016, pp. 1593-1601.
doi: 10.2514/1.g000258

[17] Slater, G. L., Byram, S. M., and Williams, T. W. "Collision Avoidance for Satellites in Formation Flight," *Journal of Guidance, Control, and Dynamics*, Vol. 29, No. 5, 2006, pp. 1140-1146.
doi: 10.2514/1.16812

[18] Wen, C., and Gurfil, P. "Relative Reachable Domain for Spacecraft with Initial State Uncertainties," *Journal of Guidance, Control, and Dynamics*, Vol. 39, No. 3, 2016, pp. 462-473.
doi: 10.2514/1.G000721

[19] Battin, R. H. *An introduction to the mathematics and methods of astrodynamics*. New York: AIAA, 1987.

[20] Geller, D. K. "Linear covariance techniques for orbital rendezvous analysis and autonomous onboard mission planning," *Journal of Guidance Control and Dynamics*, Vol. 29, No. 6, 2006, pp. 1404-1414.
doi: 10.2514/1.19447

[21] Sabol, C., Hill, K., Alfriend, K., and Sukut, T. "Nonlinear effects in the correlation of tracks and covariance propagation," *Acta Astronautica*, Vol. 84, 2013, pp. 69-80.
doi: 10.1016/j.actaastro.2012.08.023

[22] Vittaldev, V., and Russell, R. P. "Space Object Collision Probability via Monte Carlo on the Graphics Processing Unit," *The Journal of the Astronautical Sciences*, 2017, pp. 1-25.
doi: 10.1007/s40295-017-0113-9

[23] Julier, S. J., and Uhlmann, J. K. "Unscented filtering and nonlinear estimation," *Proceedings of the IEEE*, Vol. 92, No. 3, 2004, pp. 401-422.

[24] Jones, B. A., Doostan, A., and Born, G. H. "Nonlinear Propagation of Orbit Uncertainty Using Non-Intrusive Polynomial Chaos," *Journal of Guidance Control and Dynamics*, Vol. 36, No. 2, 2013, pp. 430-444.
doi: 10.2514/1.57599

[25] Jones, B. A., Parrish, N., and Doostan, A. "Postmaneuver Collision Probability Estimation Using Sparse Polynomial Chaos Expansions," *Journal of Guidance Control and Dynamics*, Vol. 38, No. 8, 2015, pp. 1425-1437.
doi: 10.2514/1.G000595

[26] Park, R. S., and Scheeres, D. J. "Nonlinear Mapping of Gaussian Statistics: Theory and Applications to Spacecraft Trajectory Design," *Journal of Guidance, Control, and Dynamics*, Vol. 29, No. 6, 2006, pp. 1367-1375.
doi: 10.2514/1.20177

[27] Park, I., and Scheeres, D. J. "Hybrid Method for Uncertainty Propagation of Orbital Motion," *Journal of Guidance, Control, and Dynamics*, 2017, pp. 1-15.
doi: 10.2514/1.G001834

[28] Valli, M., Armellin, R., Di Lizia, P., and Lavagna, M. R. "Nonlinear Mapping of Uncertainties in Celestial Mechanics," *Journal of Guidance, Control, and Dynamics*, Vol. 36, No. 1, 2013, pp. 48-63.
doi: 10.2514/1.58068

[29] Wittig, A., Di Lizia, P., Armellin, R., Makino, K., Bernelli-Zazzera, F., and Berz, M. "Propagation of large uncertainty sets in orbital dynamics by automatic domain splitting," *Celestial Mechanics and Dynamical Astronomy*, Vol. 122, No. 3, 2015, pp. 239-261.
doi: 10.1007/s10569-015-9618-3

[30] DeMars, K. J., Bishop, R. H., and Jah, M. K. "Entropy-based approach for uncertainty propagation of nonlinear dynamical systems," *Journal of Guidance, Control, and Dynamics*, Vol. 36, No. 4, 2013, pp. 1047-1057.
doi: 10.2514/1.58987

[31] Vishwajeet, K., Singla, P., and Jah, M. "Nonlinear Uncertainty Propagation for Perturbed Two-Body Orbits," *Journal of Guidance, Control, and Dynamics*, Vol. 37, No. 5, 2014, pp. 1415-1425.
doi: 10.2514/1.g000472

[32] Vittaldev, V., and Russell, R. P. "Space Object Collision Probability Using Multidirectional Gaussian Mixture Models," *Journal of Guidance, Control, and Dynamics*, Vol. 39, No. 9, 2016, pp. 2163-2169.
doi: 10.2514/1.g001610

[33] Sun, Y., and Kumar, M. "Uncertainty propagation in orbital mechanics via tensor decomposition," *Celestial Mechanics and Dynamical Astronomy*, Vol. 124, No. 3, 2015, pp. 269-294.
doi: 10.1007/s10569-015-9662-z

[34] Sun, Y., and Kumar, M. "Uncertainty forecasting in the perturbed two-body problem via tensor decomposition," *2016 American Control Conference (ACC)*. IEEE, Boston, MA, USA, 2016, pp. 5431-5436.

[35] Fujimoto, K., and Scheeres, D. J. "Tractable Expressions for Nonlinearly Propagated Uncertainties," *Journal of Guidance, Control, and Dynamics*, Vol. 38, No. 6, 2015, pp. 1146-1151.
doi: 10.2514/1.g000795

[36] Yang, Z., Luo, Y. Z., and Zhang, J. "Nonlinear Semi-Analytic Uncertainty Propagation of Trajectory under Impulsive Maneuvers," *Journal of Guidance, Control, and Dynamics*, 2017.

[37] Vittaldev, V., Russell, R. P., and Linares, R. "Spacecraft Uncertainty Propagation Using Gaussian Mixture Models and Polynomial Chaos Expansions," *Journal of Guidance, Control, and Dynamics*, Vol. 39, No. 12, 2016, pp. 2615-2626.
doi: 10.2514/1.g001571

[38] Luo, Y.-z., and Yang, Z. "A review of uncertainty propagation in orbital mechanics," *Progress in Aerospace Sciences*, Vol. 89, 2017, pp. 23-39.
doi: 10.1016/j.paerosci.2016.12.002

[39] Lee, S., and Hwang, I. "Analytical Solutions to Uncertainty Propagation in Satellite Relative Motion," *AIAA Guidance, Navigation, and Control (GNC) Conference*. American Institute of Aeronautics and Astronautics, Boston, MA, 2013.

[40] Bierbaum, M. M., Joseph, R. I., Fry, R. L., and Nelson, J. B. "A Fokker-Planck model for a two-body problem," *Bayesian Inference and Maximum Entropy Methods in Science and Engineering*. Vol. 617, American Institute of Physics Publishing, Baltimore, Maryland, 2001, pp. 340-371.

[41] Yang, Z., Luo, Y.-Z., Zhang, J., and Tang, G.-J. "Uncertainty Quantification for Short Rendezvous Missions Using a Nonlinear Covariance Propagation Method," *Journal of*

Guidance, Control, and Dynamics, Vol. 39, No. 9, 2016, pp. 2170-2178.
doi: 10.2514/1.G001712

[42] Vallado, D. A., and Alfano, S. "Curvilinear coordinate transformations for relative motion," *Celestial Mechanics and Dynamical Astronomy*, Vol. 118, No. 3, 2014, pp. 253-271.
doi: 10.1007/s10569-014-9531-1

[43] Coppola, V. T., and Tanygin, S. "Using Bent Ellipsoids to Represent Large Position Covariance in Orbit Propagation," *Journal of Guidance, Control, and Dynamics*, Vol. 38, No. 9, 2015, pp. 1775-1784.
doi: 10.2514/1.g001011

[44] Alfriend, K. T., and Yan, H. "Evaluation and Comparison of Relative Motion Theories," *Journal of Guidance, Control, and Dynamics*, Vol. 28, No. 2, 2005, pp. 254-261.
doi: 10.2514/1.6691